GLOBAL BIOGEOCHEMICAL CYCLES, VOL. 12, NO. 3, PAGES 479-499, SEPTEMBER 1998

Meridional transport of dissolved inorganic carbon in the South Atlantic Ocean

J. Holfort,[1,2] K. M. Johnson,[1] B. Schneider,[3] G. Siedler,[4] and D. W. R. Wallace [1,2]

Abstract. The meridional oceanic transports of dissolved inorganic carbon and oxygen were calculated using six transoceanic sections occupied in the South Atlantic between 11°S and 30°S. The total dissolved inorganic carbon (TCO_2) data were interpolated onto conductivity-temperature-depth data to obtain a high-resolution data set, and Ekman, depth-dependent and depth-independent components of the transport were estimated. Uncertainties in the depth-independent velocity distribution were reduced using an inverse model. The inorganic carbon transport between 11°S and 30°S was southward, decreased slightly toward the south, and was -2150 ± 200 kmol s^{-1} (-0.81 ± 0.08 Gt C yr^{-1}) at 20°S. This estimate includes the contribution of net mass transport required to balance the salt transport through Bering Strait. Anthropogenic CO_2 concentrations were estimated for the sections. The meridional transport of anthropogenic CO_2 was northward, increased toward the north, and was 430 kmol s^{-1} (0.16 Gt C yr^{-1}) at 20°S. The calculations imply net southward inorganic carbon transport of 2580 kmol s^{-1} (1 Gt C yr^{-1}) during preindustrial times. The slight contemporary convergence of inorganic carbon between 10°S and 30°S is balanced by storage of anthropogenic CO_2 and a sea-to-air flux implying little local divergence of the organic carbon transport. During the preindustrial era, there was significant regional convergence of both inorganic carbon and oxygen, consistent with a sea-to-air gas flux driven by warming. The northward transport of anthropogenic CO_2 carried by the meridional overturning circulation represents an important source for anthropogenic CO_2 currently being stored within the North Atlantic Ocean.

1. Introduction

As high-quality data on the global distribution of CO_2 in the atmosphere became available, it became possible to combine these data with atmospheric transport models to infer the transport of CO_2 from one part of the globe to another [e.g., *Keeling et al.*, 1989; *Tans et al.*, 1990; *Enting et al.*, 1995]. This approach promises to provide insight into the regional distribution of sources and sinks of atmospheric CO_2; however, to be useful in analyzing the global carbon cycle, such an analysis requires an assessment of the corresponding transport of CO_2 by the ocean circulation [*Broecker and Peng*, 1992].

The oceanic transport of chemical properties can be approached using methods similar to those developed for the calculation of heat and water transports [e.g., *Wunsch*, 1978; *Hall and Bryden*, 1982; *Roemmich and Wunsch*, 1985]. This approach has been applied to the transport of nutrients [*Rintoul and Wunsch*, 1991; *Wunsch et al.*, 1983; *Robbins and Bryden*, 1994] and inorganic carbon [*Brewer et al.*, 1989; *Martel and Wunsch*, 1993; *Robbins*, 1994; *Holfort et al.*, 1994; *Stoll et al.*, 1996]. The latter made use of measurements of the total dissolved inorganic carbon content of seawater (TCO_2).

Some of these analyses of inorganic carbon transports have been limited by a lack of high-quality, densely sampled sections with TCO_2 measurements, as well as by incomplete specification of the various components of the transport which can contribute to the meridional transport of CO_2. Densely sampled, high-quality TCO_2 data are, however, now being collected in conjunction with World Ocean Circulation Experiment (WOCE) cruises, by the Joint Global Ocean Flux Study (JGOFS) global survey of CO_2 in the oceans [*Sabine et*

[1]Department of Applied Science, Brookhaven National Laboratory, Upton, New York.
[2] Now at Institut für Meereskunde an der Universität Kiel, Kiel, Germany.
[3]Sektion Meereschemie, Institut für Ostseeforschung, Rostock-Warnemünde, Germany.
[4]Institut für Meereskunde an der Universität Kiel, Kiel Germany.

Paper number 98GB01533.
0886-6236/98/98GB-01533$12.00

al., 1997]. An example of the use of transport estimates calculated using modern section data was recently reported by *Stoll et al.* [1996].

In this paper, we use a set of these new WOCE sections, with corresponding TCO_2 data, as the basis for calculating the north-south transport of CO_2 within the South Atlantic Ocean (we also report the transport of dissolved oxygen). We focus a great deal of attention on the uncertainties which inevitably arise in such calculations. The calculations we present are appropriate for the early 1990s when the observations were made. However, the concentration of CO_2 in the oceans is increasing with time as a result of the uptake of excess or anthropogenic CO_2 from the atmosphere, and anthropogenic CO_2 concentrations and ocean currents are both spatially variable. We therefore also estimated the concentration distribution of anthropogenic CO_2 in the sections and calculated its transport. On the assumption that the ocean circulation and the ocean's natural carbon cycle have not changed significantly since preindustrial times (e.g., since 1750), subtraction of the anthropogenic CO_2 transport from the total transport measured in the early 1990s provides an estimate of the inorganic carbon transport which occurred during preindustrial times. In a separate paper, we will discuss the implications of the anthropogenic CO_2 transport for the storage of anthropogenic CO_2 in the North Atlantic Ocean.

2. Data and Data Interpolation

The main hydrographic sections used for the calculation of the meridional transport of inorganic carbon in the South Atlantic were the WOCE sections A8 (11°S), A9 (~19°S) and A10 (~30°S). These sections were occupied by the Institut für Meereskunde, Kiel, Germany, on board the research vessel *Meteor* between 1991 and 1994 [*Siedler and Zenk*, 1992 ; *Siedler et al.*, 1993; *Zenk and Müller*, 1995; *Siedler et al.*, 1996]. The total dissolved inorganic carbon (TCO_2) values [*Johnson et al.*, 1995, 1998] were determined using single-operator multiparameter metabolic analyzer systems [*Johnson and Wallace*, 1992; *Johnson et al.*,1993]. On the WOCE cruises, the TCO_2 analyses were cross-checked for accuracy against Certified Reference Materials provided by A. Dickson of Scripps Institution of Oceanography. These analyses suggested that the WOCE data are accurate to better than 2 μmol kg^{-1}. Additional sections were taken from historical data, particularly the high-quality pre-WOCE TCO_2 data collected during the South Atlantic Ventilation Experiment (SAVE) (T. Takahashi and D. Chipman, personal communication, 1991). We have compared the data from SAVE Legs 2 and 3 in the Western Basin with the the WOCE TCO_2 data from the same region using a multivariate approach and found no significant offsets between the data sets [*Wallace et al.*, 1996]. Table 1 presents a summary of the sections used, and Figure 1 shows their geographical locations.

In order to calculate material transports from hydrographic section data, high data densities are generally required. Water chemistry data are available for a maximum of ~36 discrete depths per station (> 100 m resolution), compared to the ~2 dbar resolution of the conductivity-temperature-depth (CTD) profiler data from which geostrophic water transports are estimated. Although nutrients, oxygen, and the CTD data are available for almost all of these bottle samples, TCO_2 measurements are not available for every station and every bottle depth because of analysis time limitations. To increase the TCO_2 data density prior to making the inorganic carbon transport calculations, some form of interpolation or mapping scheme is required. Recently, *Goyet et al.* [1995] demonstrated the potential of quadratic spatial interpolation of sparse TCO_2 data. As they noted, however, consideration of near-continuous profiles of "master variables" such as T, S, and O_2 should allow significant improvement over spatial interpolation schemes. Previous studies which used multiple linear regression with such variables to interpolate TCO_2 onto bottle data were performed on basin scales [*Brewer et al.*, 1995;

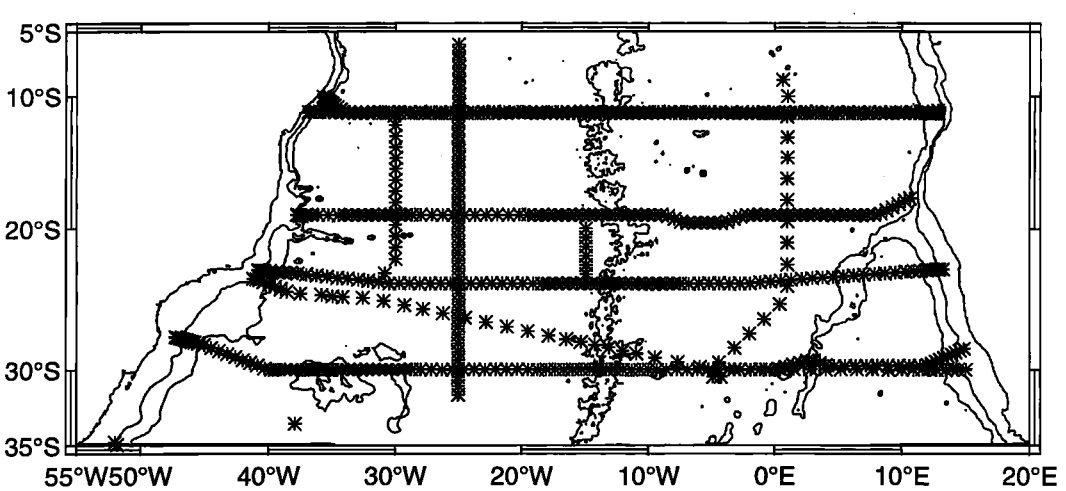

Figure 1. Map of the South Atlantic Ocean showing the geographical positions of the geostrophic velocities used in the transport calculations. Each star represents a location midway between two adjacent stations. Please note that there are overlapping sections at 11°S and toward the eastern end of 30°S (east of 5°W). The meridional sections are used only with the conservation constraints in the inverse model (see appendix, constraint B).

Table 1. Section Data Used for this Study

Cruise	WOCE Section	Date	Location (s)	Bottles Tripped	TCO_2 Samples	Institutions
Meteor 28	A8	April 1994	11°S	3840	1540	IfM / BNL
Meteor 15	A9	February 1991	19°S	3290	690	IfM / BNL
Meteor 22	A10	January 1993	30°S	3420	1420	IfM / BNL
Oceanus 133	-	March 1983	11°S, 23°S	3690	0	WHOI
SAVE Leg 3	-	February 1988	25°S, 0°W	2560	1620	SIO/LDEO
SAVE Leg 4	-	December 1988	30°S	2290	1040	SIO/LDEO

"Bottles Tripped" refers to all water samples collected during the cruise, of which only a subset were analyzed for TCO_2. Note that the Oceanus sections were not sampled for TCO_2: values were interpolated using the method described in the text on the basis of adjacent section data. These sections were used because the transport estimates are highly contingent on the mass transport fields: hence we used all available sections. Abbreviations are as follows: IfM, Institute fur Meereskunde, Kiel; BNL, Brookhaven National Laboratory; WHOI, Woods Hole Oceanographic Institution; SIO, Scripps Institute of Oceanography; and LDEO, Lamont-Doherty Earth Observatory. Dash indicates non-WOCE cruises.

Wallace, 1995]. The residuals for such large-scale regressions vary systematically with geographic position and depth [*Wallace*, 1995].

We therefore developed a three-step procedure to map the sparse TCO_2 bottle data onto the CTD data using multiple linear regression. Our approach involved the development of localized multiparameter linear regressions from all the available bottle data which were located within a specified domain centered around the position (latitude, longitude, pressure, or depth) at which a value was to be calculated. A horizontal domain extent of 2° x 2° was chosen to provide an adequate number of samples for each domain in most cases. The vertical extent of the regression domains (2 x ΔP_{reg}) was varied with pressure, starting at ± 150 dbar around the desired position close to the sea surface and increasing with depth according to

$$\Delta P_{reg} = 150 + 0.1 * P \qquad (1)$$

where P is the pressure. A variable vertical extent was required because of the stronger vertical gradients found in the upper ocean and the lower resolution of the bottle data at greater depths. In cases where there were insufficient bottle data to constrain a regression fit for a domain of this size, the size of the domain was doubled. This was necessary for the *Oceanus* cruises, on which no TCO_2 measurements were made and for which the mapping onto the bottle and CTD data relied on regression equations derived from data collected from adjacent cruise tracks. A 5° x 5° area was used for the *Meteor* 15 (19°S) cruise for which the data density was relatively sparse.

In step 1, we first used multiple linear regression to calculate the few missing nutrient data within the bottle data sets. We subsequently estimated TCO_2 values for all of the bottle samples for which there was no TCO_2 analysis. The latter was achieved using regressions with the following independent parameters: apparent oxygen utilization (AOU), NO_3, SiO_4, salinity (S), and potential temperature (Θ). A rationale for the choice of these predictor variables is given by *Brewer et al.* [1995] and *Wallace* [1995]. Figure 2 presents a composite plot of the residuals for the TCO_2 data derived from these regressions for one of the zonal sections used in this study. The standard deviation of the residuals from these fits for all TCO_2 data is 3 μmol kg^{-1}, with a tendency for larger residuals within the upper 200 m (Figure 2) [cf. *Brewer et al.*, 1995]. The now "complete" bottle data set for TCO_2 was used in step 2 to interpolate the nutrients and TCO_2 fields onto the CTD measurements. For every CTD depth (2 dbar resolution), a regression with independent variables AOU, S, Θ, and σ_Θ was performed using the bottle data that were located within the local domain (as defined above) centered on the particular CTD depth. Finally, the local regression equations were applied to the CTD profile data to estimate a TCO_2 concentration for each depth in the CTD record. Using this three-step method, we attained an effective TCO_2 data density of ~50 km horizontal resolution along the cruise tracks and 2-10 dbar in the vertical (the relatively slow response of the oxygen sensor likely reduces the effective vertical resolution of the CTD-O_2 measurements). A similar approach has been recently proposed by *Goyet and Davis* [1997]; the principal difference is our use of geographically localized regressions throughout the water column.

3. Method

The method for calculating the CO_2 transport was similar to that used previously for the calculation of heat and salt transports and was based on techniques introduced by *Bryan* [1962], *Wunsch* [1978], *Roemmich* [1980], etc. for the North Atlantic. Closely related calculations using South Atlantic data have been performed by *Fu* [1981], *MacDonald* [1993], *Holfort* [1994], *Saunders and King* [1995] and J. Holfort et al. (The heat transport in the South Atlantic Ocean, manuscript in preparation, 1998; hereinafter referred to Holfort et al., manuscript in preparation 1998). In particular, *Holfort*

[1994] and Holfort et al. (manuscript in preparation, 1998) presented calculations of heat and freshwater transports for the same sections discussed here, together with a more detailed discussion of the calculation procedures. It is worth noting that the heat transports calculated from the sections discussed here agree very well with those estimated by other workers for similar latitude ranges. These have been summarized and placed in a global and historical context by *MacDonald and Wunsch* [1996].

We use the term inorganic carbon transport (T_C) for the net transport of TCO_2 across an ocean section, that is,

$$T_c = \int_{Am}^{Af} \int_{-H}^{0} v . \varrho_{S,T,P} . TCO_2 \; dx\,dz \qquad (2)$$

The T_C was calculated by integrating the product of total inorganic carbon (TCO_2) with the in-situ density ($\rho_{S,T,P}$) and the velocity (v) that is orthogonal to the section, from the American (Am) to the African (Af) continent over the entire water column (i.e., to the bottom depth, - H). Because we had discrete station spacing, the integral was replaced with a sum over station pairs. It was assumed that the ocean is in geostrophic balance except for a directly wind-driven Ekman velocity. Two alternative approaches to defining the velocity field were used: a level-of-no-motion approach and an inverse model approach.

3.1. Level-of-No-Motion Approach

For computational reasons associated with different constraints used for the calculation of heat transport (which assumes zero net mass transport across a section) and salt/carbon/mass transport (in which a nonzero salt transport constraint is invoked), the velocity field was broken down into several components. This decomposition also facilitated sensitivity studies that examined sources of uncertainty in the inorganic carbon transport estimates. The velocity at any location on a section was

$$v(x,z) = v'(x,z) + \left[v^{EK}(x,z) - \bar{v}^{EK}_{\cdot comp} \right] + \left[\bar{v}^{LNM}(x) - \bar{v}^{LNM}_{\cdot comp} \right] + \bar{v}^{S} \qquad (3)$$

where $v'(x,z)$ is the "baroclinic" velocity which can be calculated directly from the hydrographic data and is defined so that for each station pair

$$\int_{-H}^{0} v' \, dz = 0 \qquad (4)$$

and v^{EK} is the Ekman layer velocity for each station pair, which was assumed to be distributed evenly through the upper 50 m of the water column and to be zero below that. It was calculated from *Hellermann and Rosenstein*'s [1983] climatological average wind stress data. The integrated Ekman transport over the entire section was then mass compensated by a spatially uniform, depth-independent velocity in order that this component of the transport gave zero net mass transport across the section. The compensating velocity was defined as

$$\bar{v}^{EK}_{\cdot comp} = \frac{\int_{Am}^{Af} \int_{-H}^{0} v^{EK} \varrho_{S,T,P} \; dx\,dz}{\int_{Am}^{Af} \int_{-H}^{0} \varrho_{S,T,P} \; dx\,dz} \qquad (5)$$

The depth-independent or "barotropic" velocity $\bar{v}^{LNM}$ was specified on the basis of an assumed level of no motion (LNM). For the simplest LNM choice considered, the "baroclinic" case, this barotropic component was specified to be zero for each station pair (see (4)). However, we employed 34 additional approaches to specifying a level of no motion [*Holfort*, 1994]. Briefly, these approaches included (1)

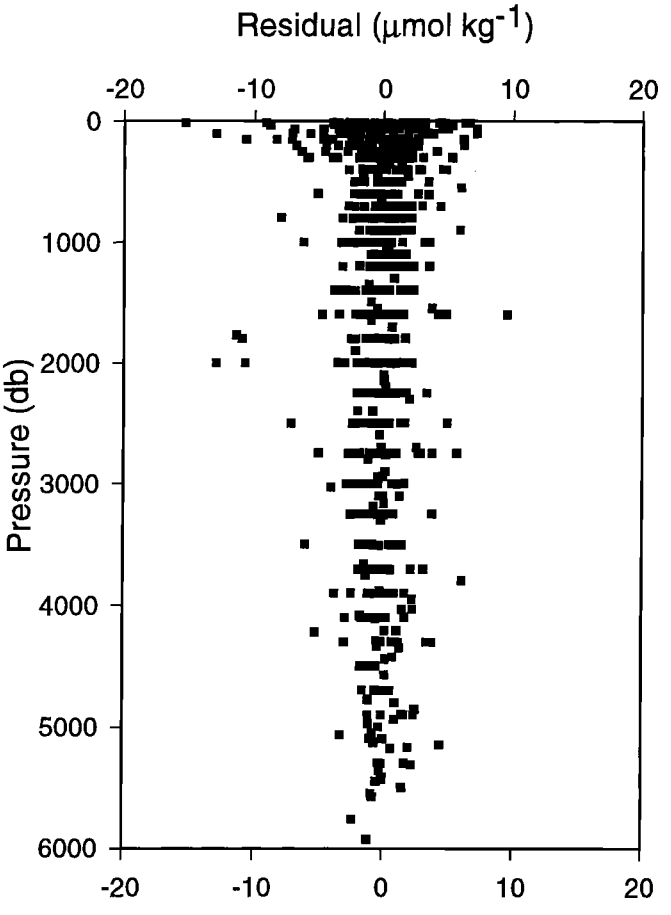

Figure 2. The difference between the TCO_2 concentration as measured on water samples collected during *Meteor* 15 (19°S) and that predicted using the multiple linear regression approach described in the text for step 1 of the data interpolation procedure. For this cruise, missing nutrient data were first interpolated using a multiple linear regression using a horizontal domain of 2°x 2°. The relatively sparse TCO_2 data set for this cruise required a larger interpolation domain of 5° x 5°.

use of a fixed horizontal pressure level for the entire section (we used levels which were varied systematically every 400 dbar between the surface and 5200 m); (2) selection of certain key isopycnals and isotherms; and (3) use of a geographically variable level of no motion derived from a water mass analysis. One particular specification of this type was used for several subsequent calculations and is referred to as LNM-2. Details concerning this specification are given by Holfort et al. (manuscript in preparation, 1998). The $\bar{v}^{LNM}$ field derived from the level-of-no-motion choice was subsequently adjusted in order that there be zero net mass transport across the entire section arising from this component of the transport. This "compensating" velocity was defined as

$$\bar{v}^{LNM}_{\cdot comp} = \frac{\int_{Am}^{Af}\int_{-H}^{0} \bar{v}^{LNM}.\varrho_{S,T,P}\,dx\,dz}{\int_{Am}^{Af}\int_{-H}^{0} \varrho_{S,T,P}\,dx\,dz} \qquad (6)$$

As with the Ekman transport mass compensation, this adjustment velocity was distributed uniformly across the entire section. Note that the barotropic mass transport compensation required to satisfy the zero-net-mass transport constraint could be quite large. However, when this was distributed uniformly across an entire section, the large cross-sectional area involved (section ~5000 km wide by ~5 km deep) implied that the corresponding barotropic velocity adjustments were too small to be directly measurable (of the order of 0.001 m s^{-1}).

Finally, an extra, spatially uniform, barotropic velocity component, $\bar{v}^{S}$, was specified in order to force the net salt transport across the section to match the net transport of salt which enters the Atlantic through the Bering Strait. Evaporation, precipitation, and runoff, because they involve freshwater, have a negligible effect on the mass of salt contained within the ocean (even though such processes alter the salinity via dilution and concentration). Therefore, if a steady state salt content of the Atlantic Ocean is being maintained, the amount of salt which enters the Atlantic Ocean to the north through the Bering Strait must be balanced by the same amount of salt leaving the Atlantic to the south. Given a mass transport of 0.8 x 10^9 kg s^{-1} [*Coachman and Aagaard*, 1988] and a mean salinity of 32.5, the salt transport through Bering Strait is approximately 26.7 x 10^6 kg s^{-1}. This must be balanced by the meridional salt transport across our zonal sections in the South Atlantic. While the required component of the barotropic transport is very important for the overall net carbon transport across an ocean section (up to 1 x 10^9 kg s^{-1}, carrying up to 2000 kmol s^{-1}; see below), it does not necessarily contribute to a carbon transport divergence between sections. As a result, it has often not been explicitly included in prior calculations of the carbon transport. Some confusion has arisen in the literature as a result of this distinction, however (see section 7). This "extra" barotropic transport component, which was assumed to be distributed uniformly across an entire section, resulted in a net mass transport across each of the sections. The associated velocity, $\bar{v}^{S}$, was calculated from

$$\begin{aligned}\bar{v}^{S}.\int_{Am}^{Af}\int_{-H}^{0} S.\varrho_{S,T,P}\,dx\,dz &= \int_{Am}^{Af}\int_{-H}^{0} v'.S.\varrho_{S,T,P}\,dx\,dz \\ &+ \int_{Am}^{Af}\int_{-H}^{0} v^{EK}.S.\varrho_{S,T,P}\,dx\,dz \\ &- \bar{v}^{EK}_{\cdot comp}.\int_{Am}^{Af}\int_{-H}^{0} S.\varrho_{S,T,P}\,dx\,dz \\ &+ \int_{Am}^{Af}\int_{-H}^{0} \bar{v}^{LNM}.S.\varrho_{S,T,P}\,dx\,dz \\ &- \bar{v}^{LNM}_{\cdot comp}.\int_{Am}^{Af}\int_{-H}^{0} S.\varrho_{S,T,P}\,dx\,dz \\ &- T_S^{BS}\end{aligned} \qquad (7)$$

where T_S^{BS} is the salt transport through the Bering Strait.

3.2. Inverse Model Approach

In order to reduce the uncertainties and avoid some arbitrariness associated with the choice of a level of no motion, we also developed an inverse model using additional constraints to assist with the specification of the barotropic velocity field. Note that with this approach, we solved for the entire barotropic velocity for each station pair, and there was no artificial division into the three distinct barotropic components used with the level-of-no-motion approach. In the inverse analysis, the constraints are used to set up a linear equation system or "model" for the unknown velocities, and the system was then solved using singular value decomposition. This method was used by *Wunsch* [1978] in the North Atlantic, and calculations using South Atlantic data were performed by *Fu* [1981], *MacDonald* [1993], *Holfort* [1994] and Holfort et al. (manuscript in preparation, 1998). We refer the reader to these publications for detailed descriptions of the inverse method; a listing of the constraints that we employed is given in the appendix.

In performing the inverse analysis, solutions based upon many different models were explored; these different models included different formulations for the weighting of the additional constraints and data as well as the three separate variants of a phosphate transport constraint (see appendix). The sensitivity of the solutions to the initial specification of a level of no motion was also explored. The goal of such an approach is to find a set of solutions that is consistent with the constraints and the data to within a specified stringency. An exact solution to the imposed constraints is generally not desired because the constraints are themselves not an exact representation of the ocean's behavior and have uncertainties, as do the data. At high matrix rank, which corresponds to a stringent specification of the constraints, such errors and uncertainties tend to be magnified, resulting in unreasonably high and variable barotropic velocities. At low matrix rank, the solution will be out of the range of the uncertainty of the data and/or constraints, and the solution therefore can be

judged incorrect. Our goal was to find a set of solutions that satisfied the constraints within reasonable error margins. It should therefore be remembered that there is no unique or "correct" solution, but there is rather a range of different solutions that depend on the rank and the particulars of the model including its initial state and factors such as the weighting and scaling of the various equations and unknowns.

4. Results and Uncertainties

4.1. Overview of the Inorganic Carbon Transport

In order to set the context for subsequent discussion of uncertainties in the carbon transport estimates, we first summarize the results from our analysis of the data. Throughout we use the convention that positive numbers refer to northward transport. In the following, T refers to transport estimates (with T_C referring to carbon, and T_M referring to mass). C denotes the concentration of total dissolved inorganic carbon. Superscripts are used to distinguish the different components of the transport (see section 3): EK refers to the mass-compensated Ekman component, BC the baroclinic component, S refers to the net mass transport component required to satisfy the salt transport constraint, and LNM refers to the mass-compensated barotropic component associated with the choice of a level of no motion. Angled brackets ($<>$) denote an averaged quantity. Carbon transports are reported in kmol s^{-1} (1 Gt C yr^{-1} = 1 Pg C yr^{-1} = 2642 kmol s^{-1}).

The overall best estimate for the meridional inorganic carbon transport (T_C) in the South Atlantic Ocean, between 11°S and 30°S, was of the order of -2150 kmol s^{-1} (i.e., southward). This estimate, which was derived from the inverse modeling approach, applies to T_C at the time of the measurements: the early-to-middle 1990s. Using the level-of-no-motion approach described in section 3, we can view the T_C across each section as being carried by the four main mass transport components listed above: T^{BC}, T^{EK}, T^{LNM}, and T^S. Using the results of the analyses presented in Tables 2, 3, and 4, it is possible to distinguish their relative contributions to T_C.

Table 2 indicates that at 11°S, there was a large southward Ekman mass transport (T_M^{EK}) per se within the upper 50 m of the water column, carrying the TCO_2 concentration of this upper layer (C^{EK}). The (southward) carbon transport in this layer was therefore very large (-12 x 10^9 kg s^{-1} x 2055 μmol kg^{-1}) or -24,660 kmol s^{-1}. However this is offset by the northward mass-compensating barotropic transport which carries the higher concentration characteristic of the water column average ($<C>$). The compensating transport carried (+12 x 10^9 kg s^{-1} x 2196 μmol kg^{-1}) or +26,352 kmol s^{-1}. Hence the net carbon transport attributable to this component (T_C^{EK}) was directed northward at +1700 kmol s^{-1}.

Table 3 presents results calculated using the "baroclinic" choice of LNM (see (4)). The (southward) T_C of -1903 kmol s^{-1} at 11°S includes the contribution from T_C^{EK} discussed in the previous paragraph, as well as from T_C^S. The latter carries (-0.92 x 10^9 kg s^{-1} x 2196 μmol kg^{-1}) or -2020 kmol s^{-1} (Tables 2 and 4). Hence the transport of carbon associated with the baroclinic structure of the velocity field (T_C^{BC}) at 11°S is (-1903 - 1700 +2020) or -1583 kmol s^{-1}. Use of a more sophisticated LNM choice (LNM-2) gave a somewhat larger value for T_C of -2345 kmol s^{-1} (Table 3). A difference between this value and T_C using the "baroclinic" choice of LNM (Table 3) of -442 kmol s^{-1} reflects a small additional barotropic contribution to the net carbon transport (T_C^{LNM}). Hence at 11°S, T_C^{BC} and T_C^{EK} are both significant but can be viewed as roughly balancing each other so that the net carbon transport T_C is carried primarily by the net mass transport across the section (T_C^S).

At 30°S, the Ekman mass transport is much smaller, and T_C^{EK} is a negligible +35 kmol s^{-1} of inorganic carbon (northward). At this latitude, the T_C^S was (-0.53 x 10^9 kg s^{-1} x 2189 μmol kg^{-1}) or -1160 kmol s^{-1} of inorganic carbon. The baroclinic component, T_C^{BC}, was therefore (-3758 - 35 + 1160) or -2633 kmol s^{-1}. Use of the more sophisticated LNM (LNM-2, Table 3) reduced the overall T_C value to -2720 kmol s^{-1} reflecting an additional barotropic component (T_C^{LNM}) of +1038 kmol s^{-1}. Hence at this latitude, the mass-compensated Ekman (T_C^{EK}) and the combined barotropic (T_C^{LNM} + T_C^S) contributions to the net carbon transport were both small so that T_C was dominated by the baroclinic circulation component (T_C^{BC}).

With this approximate breakdown in mind, we now examine the uncertainty in the carbon transport which arises from uncertainties in the specification of the different formal components of the transport (mass-compensated Ekman, baroclinic, net mass transport as well as the detailed specification of the barotropic velocity field).

4.2. Ekman Transport

For the purpose of illustrating potential errors associated with specification of the Ekman transport, we use the level-of-no-motion approach which views the mass-compensating transport as a zonally uniform barotropic mass transport (see section 3). We note below that this approach may give a worst-case view of the transport uncertainties compared to, for example, the inverse model approach. The mass-compensated Ekman component of the total carbon transport across the section (T_C^{EK}) can be approximated by

$$T_C^{EK} = T_M^{EK}.(<C^{EK}> - <C>) \qquad (8)$$

where $<C>$ and $<C^{EK}>$ are average TCO_2 concentrations of the entire section and the Ekman layer, respectively. (Note that in our full calculations, we resolved C^{EK} and T_M^{EK} for each station pair.)

Table 2 presents values for the variables in (8) for the six sections used in this study. As noted earlier, the net Ekman contribution is approximately +1700 kmol s^{-1} at 11°S and close to zero at 30°S. The concentration difference in (8) remains at about 140 μmol kg^{-1} for all of the sections, and the variation in T_C^{EK} from one section to another is therefore almost exclusively a function of the Ekman mass transport (T_M^{EK}, see Table 2).

There is considerable uncertainty concerning the magnitude of T_M^{EK} arising from uncertainties in wind stress data. For comparison, the largest differences of mean zonal wind stress in the North Atlantic between the data sets of *Hellermann and Rosenstein* [1983] and *Isemer and Hasse* [1985] are of the

Table 2. Values of the Mass-Compensated Ekman Mass Transport (T_M^{EK}), the Mean TCO_2 Concentration for the Ekman Layer ($<C>^{EK}$) and the Entire Section ($<C>$), and the Net Carbon Transport Associated with the Mass-Compensated Ekman Transport (T_C^{EK}) for Sections at Various Latitudes.

Cruise	Latitude, deg S	T_M^{EK}, 10^9 kg s^{-1}	$<C>^{EK}$, μmol kg^{-1}	$<C>$, μmol kg^{-1}	T_C^{EK}, kmol s^{-1}
Meteor 28	11	-11.8	2057	2196	+1672.
Oceanus 133	11	-12.0	2053	2196	+1744.
Meteor 15	19	-6.3	2071	2193	+785.
Oceanus 133	23	-3.8	2057	2188	+503.
SAVE Leg 3/4	25	-1.5	2047	2190	+231.
Meteor 22	30	-0.4	2046	2189	+35.

Transports are positive northward.

Table 3. Sensitivity of Carbon Transport Estimates to Uncertainties in Ekman Transport and to the Spatial Resolution of the Section Data.

Choice of Level of No Motion	Model Parameters				Transports (T_C), kmol s^{-1}		
	H^{EK} m	τ adjust	Resolution		*Meteor* 28 11°S	*Meteor* 15 19°S	*Meteor* 22 30°S
			Vertical	Horizontal			
Uncertainties in Ekman Transport							
Baroclinic	50	-	1	1	-1903	-2741	-3758
Baroclinic	20	-	1	1	-1903	-2734	-3761
Baroclinic	100	-	1	1	-2045	-2793	-3762
Baroclinic	50	-0.2	1	1	-989	-2223	-3417
Baroclinic	50	+0.2	1	1	-2816	-3259	-4100
Baroclinic	50	SOC	1	1	-2594	-3026	-3793
Spatial Resolution of the Section Data							
Baroclinic	50	-	1	1	-1903	-2741	-3758
Baroclinic	50	-	1	0.5	-2034	-2862	-3805
LNM-2	50	-	1	1	-2345	-2317	-2720
LNM-2	50	-	1	0.5	-2423	-2562	-3162
LNM-2	50	-	NODC	1	-2186	-2932	-2884
LNM-2	50	-	NODC	0.5	-2151	-2956	-3620
LNM-2	50	-	Met25	1	-2545	-2865	-2838
LNM-2	50	-	Met25	0.5	-2574	-3110	-3302
LNM-2	50	-	Met25	0.33	-3030	-3642	3545

H^{EK} is the assumed depth of the Ekman layer; "τ adjust" refers to adjustments (dynes cm^{-2}) to the *Hellermann and Rosenstein* [1983] wind stress data; "SOC" refers to the altenative wind stress climatology from the Southampton Oceanography Center (see text); horizontal resolutions of 0.5 and 0.33 refer to subsampling of sections using every second and every third station, respectively. Results for three different vertical resolutions are presented: 1 (full 2 m resolution), NODC (standard bottle depths of the National Oceanographic Data Center as of 1988), and Met25 (standard bottle depths used during the historic *Meteor* expeditions of 1925 and 1927).

order of 30% (i.e., 0.3 dyn cm^{-2} at 15°N). On the basis of the North Atlantic comparison, we estimated the uncertainty in T_C^{EK} using an assumed error in wind stress of ± 0.2 dyn cm^{-2}. Examples of the sensitivity of the total carbon transport to this uncertainty for three of the sections are presented in Table 3. T_M^{EK} is a function of the wind stress (τ) and the Coriolis parameter:

$$T_M^{EK} = \frac{\tau}{f} \tag{9}$$

Hence for a given uncertainty in wind stress (τ), the uncertainty in T_C is much greater at 11°S (±50% or 900 kmol s^{-1}, Table 3) than at 30°S (±10% or 400 kmol s^{-1}, Table 3) as a result of the variation of the Coriolis parameter f with latitude. Use of an alternative wind stress climatology from the Southampton Oceanography Center [*Josey et al.*, 1996; (see also www.soc.soton.ac.uk/JRD/MET/fluxclimatology.html) S. A. Josey et al., New insights into the ocean heat budget closure problem from analysis of the SOC air-sea flux climatology, submitted to *Journal of Climate*, 1998] gives a southward inorganic carbon transport that is 691 kmol s^{-1} greater at 11°S, with the difference decreasing to 35 kmol s^{-1} at 30°S (Table 3).

It is worth noting that whereas carbon transports based on the level-of-no-motion approach appear very sensitive to wind stress data uncertainty, this may be an artifact of the simple approach used to specify the compensating barotropic velocity field. The sensitivity to variations of wind stress of the full inverse model results was considerably smaller. For example, at 11°S, the inverse model carbon transport varied by only about 200-300 kmol s^{-1} for the various wind stress scenarios given in Table 3. The reason for the reduced sensitivity presumably lies in the details of how the inverse model distributes the transport required to mass compensate the Ekman transport.

Another possible source of uncertainty is the choice of Ekman layer depth (H^{EK}), which influences the value of $<C^{EK}>$ in (3). Normally, we use the mean TCO_2 of the upper 50 dbar of the water column as the TCO_2 concentration for the Ekman flow; however, we also made calculations using means of the upper 20 and 100 dbar to assess the sensitivity of the carbon transport to this choice. The results presented in Table 3 suggest that the overall uncertainty associated with choosing different Ekman depths is small (< 100 kmol s^{-1}) because the change of $<C^{EK}>$ with varying Ekman depth is small. Again, the effect is negligible at 30°S due to the low Ekman mass transport at that latitude. Similarly, the uncertainties associated with an uncertainty of about 5 μmol kg^{-1} in the mapping of the TCO_2 values in the surface layer (see Figure 2) are small.

The potentially large uncertainties associated with specifying the Ekman transport imply that an important task for improving transport calculations, not only for inorganic carbon but also for heat, nutrients, etc., is to obtain better estimates of the wind stress, particularly at low latitudes.

4.3. Seasonality

The sections were collected primarily during summer months, and we used climatological average wind stress data to estimate the Ekman transport. Our calculations therefore implicitly ignore (or average) seasonal factors that might affect the carbon transport. Using data collected at the Bermuda Atlantic Time Series Site as an example, seasonal changes of TCO_2 concentration of the order of 40 μmol kg^{-1} can occur in the oligotrophic ocean with this variability most pronounced in the upper 50 m - 75 m of the water column [*Bates et al.*, 1996]. At 11°S, where the surface layer mass transport is strongest (about 10 x 10^9 kg s^{-1}) due to strong Ekman transport, variability of this magnitude could translate into seasonal T_C variability of the order of 400 kmol s^{-1}. Variability at the higher-latitude sections would be smaller than this because of the smaller Ekman contribution to the transport. However, in this simple calculation we are ignoring possible seasonal covariance of upper layer TCO_2 concentrations with the Ekman transport as well as any time dependence of the non-Ekman transport. Obviously, we have a lack of data with which to reliably assess such seasonal effects, and this will be an important issue for further data collection and modeling studies.

4.4. Data Resolution

Accurate calculations of T_C from zonal sections require very close station spacing, because sums over station pairs are substituted for the integral in (2). We cannot directly estimate the error associated with this substitution. However, with a mean station spacing of ~50 km, generally closer at the boundaries and wider in the ocean interior, the main scales of motions should be resolved by our data (this was not necessarily the case with some earlier studies; see section 7). In order to provide an indication of the possible error, we "artificially"' subsampled three of the sections using every second and every third station (resolution factors of 0.5 and 0.33, respectively). We also examined the effects of vertical data resolution and combined vertical and horizontal resolution by subsampling the full section data at standard or traditional bottle sampling depths. Two variants of standard depths were used: the standard bottle depths used by the U.S. National Oceanographic Data Center as of 1988 and the standard depths employed on the historic *Meteor* cruises of 1925 and 1927. In all these reduced resolution cases, the entire velocity field was recalculated based on the "artificial" data set, and the property transports were recalculated.

The results are also presented in Table 3. The effect of halved horizontal resolution appears to be relatively minor (change in T_C of ~160 kmol s^{-1}), although a larger difference at 30°S was observed using the LNM-2 model. The effect of decreased vertical resolution also varied between sections, with a particularly large effect (~600 kmol s^{-1}) being observed at 19°S but with effects at the other sections being only 100-200 kmol s^{-1}. In general, it can be seen that, depending on the section, both horizontal and vertical data resolution changes can affect the inorganic carbon transport estimates. Table 3 shows that the combined effect of decreased vertical and horizontal resolutions can be quite significant, with changes of 700-1300 kmol s^{-1} (again dependent on the particular section examined).

4.5. Barotropic Component

A measure of the uncertainty in T_C that can arise as a result of uncertainty in the specification of the barotropic component of the velocity can be obtained from exploring the sensitivity of T_C estimates to different choices of a level of no motion (LNM). As described in section 3, we employed 35 different LNM choices. Some of the choices resulted in meridional overturning circulations that are incompatible with our knowledge of the ocean circulation. We therefore defined the circulation associated with a particular LNM choice to be "valid" if the following criteria concerning the circulation of major water masses were met: (1) the flow of Antarctic Bottom Water ($\sigma_4 > 45.92$) was northward; (2) lower North Atlantic Deep Water ($\sigma_2 > 37.07$ and $\sigma_4 < 45.92$) flowed southward; (3) the flow of upper North Atlantic Deep Water ($\sigma_2 > 36.9$ and $\sigma_2 < 37.07$) was at least 5 x 10^9 kg s^{-1} to the south; (4) the total transport of North Atlantic Deep Water was less than 26 x 10^9 kg s^{-1}; and (5) the Antarctic Intermediate Water ($26.8 < \sigma_0 < 27.4$) flowed northward.

The frequency distributions of T_C estimates resulting from the LNM choices that gave "valid" circulations are presented for the different sections as solid bars in Figure 3; the open bars represent transport estimates associated with LNM choices that gave "invalid" circulations. The mean values of T_C for the "valid" choices (Table 4) lie between ~2000 kmol s^{-1} and ~3500 kmol s^{-1} to the south, and the median values do not differ very much from these mean values. The standard

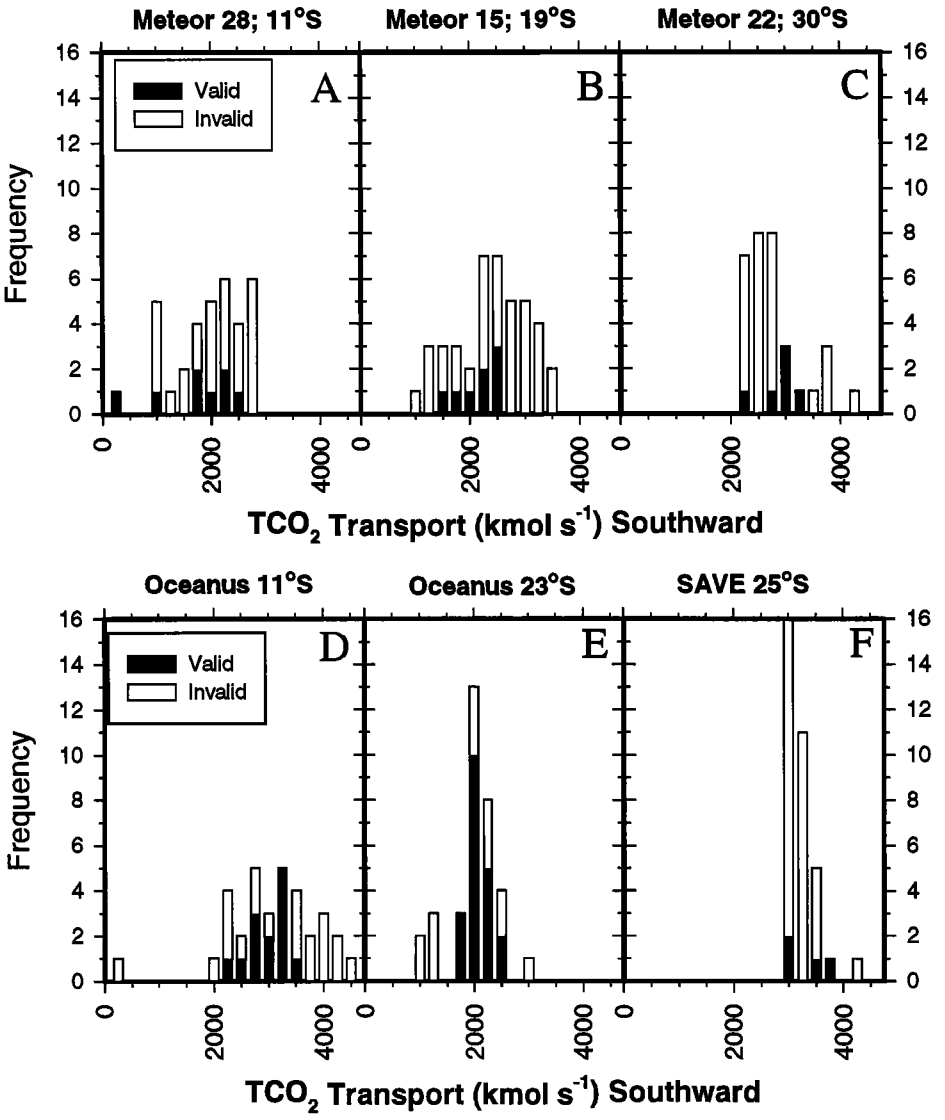

Figure 3. Frequency distributions of the T_C (in kmol s^{-1} on the x axis) for the six different zonal sections based on the level-of-no-motion approach. Solid bars represent "valid" choices of a level of no motion; open bars represent levels of no motion that resulted in an "invalid" circulation (see text for details). For these solutions, any difference between the salt transport across the section required to balance the salt transport through Bering Strait and the calculated salt transport based upon a choice of a level of no motion has been compensated for by an additional, horizontally uniform, barotropic velocity.

deviations range between 200 and 650 kmol s^{-1} with the total range (maximum-minimum) for an individual section being ~1600 kmol s^{-1}. Hence specification of a level of no motion can be a very significant source of uncertainty for the T_C estimates.

It was in order to reduce this uncertainty that we developed the inverse model analysis described in section 3. Solutions based upon many different inverse models were explored, and the sensitivity of the solutions to the initial specification of a level of no motion was also explored. A fairly consistent picture emerged: At low matrix rank, the solutions were still influenced significantly by the particular choice of initial LNM; however, at ranks of >80 this influence largely disappeared. At ranks >200, the exact nature of the constraints became important, and the effects of model and data uncertainties were amplified so that solutions for different models diverged significantly. There was a relatively stable region of carbon transport versus rank in the range 135 < rank < 165. We chose this range of solutions as the basis for the transport estimates presented in Table 4. This table presents mean transports from the inverse analysis together with estimates of the standard deviation across multiple model formulations for this range of ranks.

In general, the transports across the various sections derived from the inverse model approach are lower than the mean values derived from the level-of-no-motion approach, particularly toward the south. Examination of the solutions suggested that for the southernmost sections, it was the phosphate transport constraint that was a principal reason for the reduced transport estimate relative to those derived using the level-of-no-motion approach. The inorganic carbon transport was quasi-linearly related to the phosphate transport with a slope (ΔT_C / ΔT_{PO4}) of 110-170, where T_{PO4} is the phosphate transport. Overall, however, the uncertainty associated with the barotropic velocity specification was reduced through use of the inverse model to ~200 kmol s^{-1} for an individual section, and there was also reduced variability between the means for the individual sections.

4.6. Net Mass and Salt Transport

In order to satisfy the constraint of a total southward salt transport of 26.7 x 10^6 kg s^{-1} through the sections, our calculations require a net southward meridional mass transport of -0.96 x 10^9 kg s^{-1} at 11°S, decreasing to -0.53 x 10^9 kg s^{-1} at 30°S (see Table 4). The freshwater balance (evaporation, precipitation, and runoff) inferred from this estimate of the convergence of the mass transport agrees very well with the completely independent estimate of net freshwater fluxes for this latitude range (0.42 x 10^9 kg s^{-1}) by *Baumgartner and Reichel* [1975]. As noted earlier, assigning this net mass transport to a zonally uniform barotropic flow gives an associated inorganic carbon transport of about -2000 kmol s^{-1} at 11°S and -1160 kmol s^{-1} at 30°S due to this component of the transport alone.

The uncertainty of the T_C due to most of the sources of uncertainty in this net mass transport is already incorporated in the ranges of solutions presented in Table 4. These did not, however, consider the uncertainty in the specification of the salt transport through Bering Strait (and therefore through the South Atlantic sections). An uncertainty of 0.2 x 10^9 kg s^{-1} or

Table 4. Mean Values for Mass Transport, Inorganic Carbon Transport (T_C), Anthropogenic Carbon Transport (Ant T_C), the Preindustrial Inorganic Carbon Transport (PreInd T_C), and Dissolved Oxygen for Several Sections and Derived from Approximately 52 Separate Inverse Models per Section.

Cruise	Latitude, deg S	Inverse Model Results						LNM
		Mass	Heat	T_C	Ant T_C	Preind T_C	Oxygen	T_C
Meteor 28	11	-0.93 (0.02)	0.46 (0.09)	-2547 (213)	425 (77)	-2972 (226)	-658 (237)	-1867 (758)
Oceanus 133	11	-0.99 (0.02)	0.52 (0.09)	-1884 (272)	711 (77)	-2595 (282)	-1696 (274)	-3099 (350)
Meteor 15	19	-0.86 (0.02)	0.60 (0.07)	-2580 (214)	502 (64)	-3082 (223)	-1060 (178)	-2340 (365)
Oceanus 133	23	-0.66 (0.02)	0.32 (0.07)	-2023 (205)	322 (76)	-2345 (219)	-493 (148)	-2213 (196)
SAVE 3+4	25	-0.59 (0.04)	0.33 (0.08)	-1949 (211)	338 (92)	-2287 (230)	-429 (148)	-3472 (343)
Meteor 22	30	-0.53 (0.03)	0.27 (0.07)	-1954 (241)	291 (65)	-2245 (250)	-40 (145)	-2982 (303)

Each inverse model was initialized with the LNM-2 level of no motion (see text). The mass transports are in (10^9 kg s^{-1}), the heat transport is in units of (10^{15} W), all the carbon transports are in (kmol s^{-1}), and negative transports denote transport toward the south. Averages reflect model transports for ranks of 135 to 165 using a variety of model formulations. Numbers in parentheses reflect the standard deviation of the model transports from these various model solutions. The final column labeled "LNM" presents, for comparison, the inorganic carbon transports derived using the level-of-no-motion approach; the results are the means and standard deviations resulting from the "valid" choices of level of no motion (see text).

25% in the mass transport through Bering Strait results in an uncertainty of 6.5 x 10^6 kg s^{-1} in the salt transport which translates into an associated additional uncertainty of ~400 kmol s^{-1} for T_C in the South Atlantic. (Note that such an error would be systematic across all South Atlantic sections and therefore would not affect carbon transport divergence estimates; see section 7.)

4.7. Structure of the Transport

The quasi-vertical structure of the section-wide transports of mass, silicate, and TCO_2 for the *Meteor* 22 cruise along 30°S are presented for one typical realization of the inverse analysis in Figures 4a - 4c). Note that at this latitude, the Ekman transport is small and is included in the uppermost density layer. In these plots, the total net transport is plotted as a function of the 19 separate density intervals used in the inverse model. The corresponding density intervals are listed in the Figure 4 caption, and their depth distributions are shown in section plots (Figure 5). A three-layer system is evident in the mass transport distribution, with predominantly northward transport in the lower density layers ($\sigma_1 < 32.00$) which include the Antarctic Intermediate Water, southward transport in the middensity layers ($\sigma_1 > 32.00$ and $\sigma_3 < 41.53$) which include the North Atlantic Deep Water, and northward transport in the highest-density layers ($\sigma_3 > 41.53$) which include the lower Circumpolar Deep Water and Antarctic Bottom Water.

The carbon transport (Figure 4c) appears qualitatively very similar indicating that the overall details and magnitude of the inorganic carbon transport are controlled to first order by

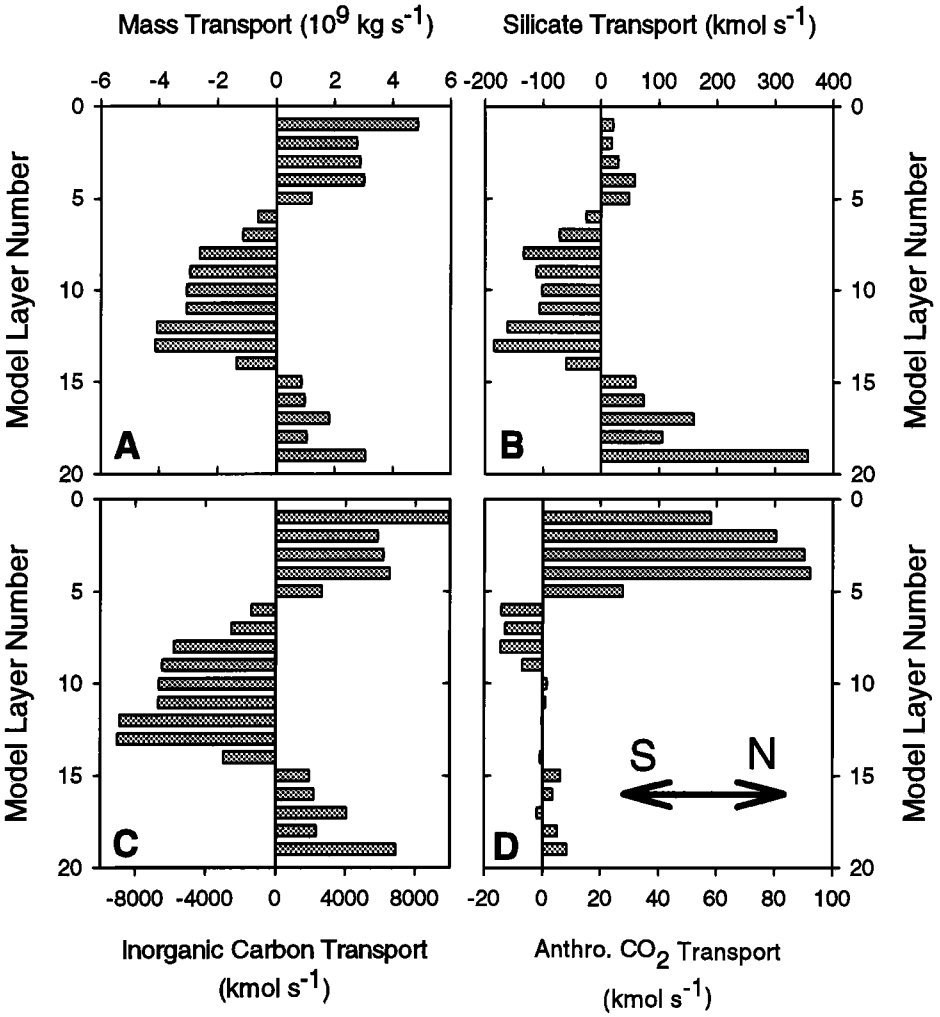

Figure 4. Vertical structure of the transport of (a) mass, (b) silicate, (c) TCO_2, and (d) anthropogenic CO_2 at 30°S (*Meteor* 22) as derived from a typical inverse model solution. Northward transport is positive. The vertical axis gives the density layer number from the inverse model. The locations of the layers are shown in section plots in Figure 5 and were defined as follows: 1, $\sigma_0 < 26.60$; 2, $26.60 < \sigma_0 < 26.80$; 3, $26.80 < \sigma_0 < 27.00$; 4, $27.00 < \sigma_0 < 27.20$; 5, $27.20 < \sigma_0$ and $\sigma_1 < 32.00$; 6, $32.00 < \sigma_1 < 32.16$; 7, $32.16 < \sigma_1$ and $\sigma_2 < 36.82$; 8, $36.82 < \sigma_2 < 36.92$; 9, $36.92 < \sigma_2 < 36.97$; 10, $36.97 < \sigma_2 < 37.00$; 11, $37.00 < \sigma_2 < 37.02$; 12, $37.02 < \sigma_2 < 37.04$; 13, $37.04 < \sigma_2$ and $\sigma_3 < 41.50$; 14, $41.50 < \sigma_3 < 41.53$; 15, $41.53 < \sigma_3$ and $\sigma_4 < 45.93$; 16, $45.93 < \sigma_4 < 45.96$; 17, $45.96 < \sigma_4 < 46.00$; 18, $46.00 < \sigma_4 < 46.02$; and 19, $\sigma_4 > 46.02$

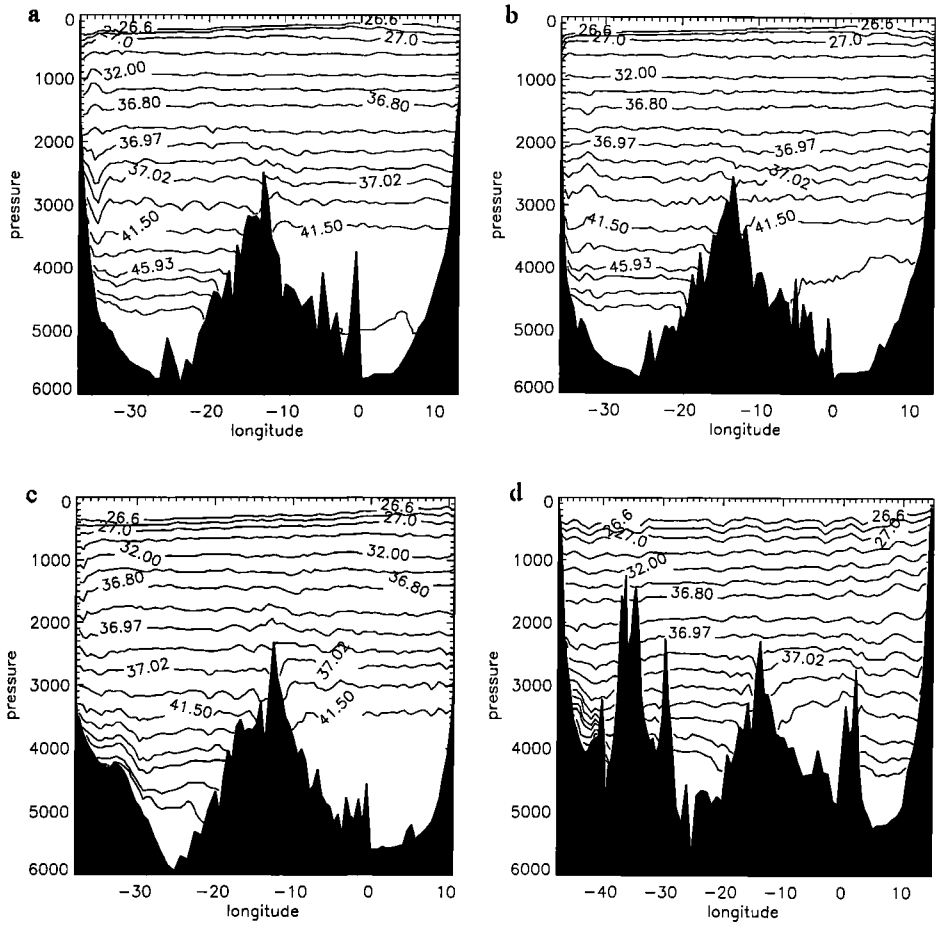

Figure 5. Distribution of the 19 layers used for the inverse model analysis in four of the sections used for this study. (a) *Oceanus* 133 at 11°S; (b) *Meteor* 28 (WOCE A8) at 11°S; (c) *Meteor* 15 (WOCE A9) at 19°S; (d) *Meteor* 22 (WOCE A10) at 30°S. In all cases, the layer number was assigned sequentially from surface to deep according to the density criteria listed in the caption to Figure 4.

variability in the mass transport and that concentration variability plays a smaller role. Conversely, the influence of vertical concentration variability is very evident in the case of the silicate transport (Figure 4b), where the effect of silicate depletion in low-density layers and very high silicate concentrations in the highest-density layer can be seen to affect the overall pattern of the transport strongly.

As with the vertical structure, the horizontal structure of the inorganic carbon transport is dependent on the mass transport distribution. The horizontal mass transport derived from the inverse model analysis is a complex subject well beyond the scope of this paper: it is covered in detail by *Holfort* [1994] and Holfort et al. (manuscript in preparation, 1998). However, the inferred circulation pattern was found to be broadly similar to that of *Reid* [1989], although some differences were also evident. At the western boundary, the southward flowing Brasil Current at 30°S (the southern boundary of the inverse model domain) was prescribed to have a transport of 10 x 10^9 kg s^{-1} (based on direct current measurements). At 11°S (our northern boundary), the mass transport showed a strong, northward flowing subsurface current which corresponds well with the combined acoustic doppler current profiler / CTD observations of *Schott et al.* [1995]. The solution also revealed a southward flow of Antarctic Intermediate Water along the western boundary at 30°S, as observed from moorings and float studies [*Boebel et al.*, 1997].

5. Anthropogenic CO_2 and the Preindustrial Transport

The estimates of T_C presented above are appropriate for the period of time during which our TCO_2 measurements were made, the early 1990s. However the concentration of dissolved inorganic carbon in the ocean is increasing with time as a result of the uptake of anthropogenic CO_2 derived from land use changes and fossil fuel burning. The near-surface concentration of TCO_2 at this latitude range has increased by ~55 μmol kg^{-1} since preindustrial times in response to the increase in atmospheric (and near-surface ocean) pCO_2 from

~275-280 μatm in 1700 [*Neftel et al.*, 1985] to ~355-358 μatm for the time of the WOCE surveys [*Conway et al.*, 1994]. It is worth considering what the oceanic transport of inorganic carbon within our study region would have been during preindustrial times. In doing this, we implicitly assume that ocean circulation patterns and rates have not changed significantly since 1750. (We note that observations of long-term changes of water properties at various locations in the ocean associated with changing atmospheric forcing [e.g., *Dickson et al.*, 1997] may prove difficult to reconcile with this assumption.)

In order to estimate T_C for the period prior to the introduction of anthropogenic CO_2 (i.e., prior to about 1750), we first estimated the anthropogenic CO_2 content of our TCO_2 data. We used a variant of calculation procedures, based upon preformed CO_2, which were introduced by *Brewer* [1978] and *Chen and Millero* [1979] and included the contribution of nitrate remineralization to alkalinity changes [e.g., *Brewer and Goldman*, 1976]. It is beyond the scope of this paper to discuss the calculation procedure in detail; however, it shared several similarities with an approach employing transient tracer data developed by *Gruber et al.* [1996]. The estimation of the anthropogenic CO_2 concentration does not contribute greatly to the overall uncertainty of either the anthropogenic or preindustrial carbon transports relative to uncertainties associated with the circulation and mass transports.

The average depth profile of anthropogenic CO_2 for each of the sections is presented in Figure 6. Very noticeable in all of the profiles is a relatively high and uniform anthropogenic CO_2 concentration in the Antarctic Intermediate Water between depths of 500 m and 1000 m. Overall, the anthropogenic CO_2 concentrations in the water column are highest toward the south, closer to the origin of the Antarctic Intermediate Water [cf. *Brewer*, 1978]. Our analysis gives a small average background level of anthropogenic CO_2 of 3-5 μmol kg^{-1} throughout the water column in each section. This nonzero background is consistent with the detection of significant levels of the anthropogenic halocarbon CCl_4 throughout the water column in the Brazil Basin and even in portions of the deep Angola Basin [*Wallace et al.*, 1994; *Roether and Putzka*, 1996]. Carbon tetrachloride has been present in the environment in significant quantities since 1920-1930 at which time the anthropogenic CO_2 content of the cold surface seawater which ventilates the deep ocean was already 12-14 μmol kg^{-1}. The anthropogenic CO_2, having been introduced since about1750, may have penetrated farther into the deep ocean than CCl_4 and considerably farther than the CFCs and bomb tracers such as ^3H and ^{14}C. Hence the finding of CCl_4 throughout most of the low- to middle-latitude South Atlantic basins suggests that no portion of the Atlantic Ocean can safely be assumed to be "free" of anthropogenic CO_2 contamination.

The anthropogenic CO_2 distributions from the section data were combined with the mass transport calculations in order to calculate the transport of anthropogenic CO_2. The resulting transport of anthropogenic CO_2 was consistently northward, with a value which ranged between 400 and 700 kmol s^{-1} at 11°S and was 300 kmol s^{-1} at 30°S. The anthropogenic carbon transports presented in Table 4 imply that the southward inorganic carbon transport T_C was ~430 kmol s^{-1} greater across 20°S during preindustrial times than it was during the early 1990s. The transport of anthropogenic CO_2 to the north arises because it is the upper ocean waters within this latitude range that contain most of the anthropogenic CO_2 , and these are moving predominantly northward (Figure 5d). Conversely, the southward return flow of "older" deeper water contains a much lower concentration of anthropogenic CO_2.

This supply of anthropogenic CO_2 to the northern and tropical Atlantic Ocean which is carried by the ocean's meridional overturning circulation is quantitatively significant relative to the uptake of anthropogenic CO_2 across the air-sea interface within the North Atlantic. For example, *Sarmiento et al.* [1995] reported a model-derived estimate of the uptake of anthropogenic CO_2 due to air-sea gas exchange within the northern Atlantic (18°S - 78°N) of ~1000 kmol s^{-1}. Our estimate of the transport of this property northward across 20°S within the ocean approaches 50% of this value. We will discuss the importance of this meridional transport for the overall budget of anthropogenic CO_2 within the North Atlantic elsewhere.

Subtraction of the anthropogenic carbon transport from T_C allows estimation of the inorganic carbon transport during preindustrial times (Table 4). The transport across 10°S was about -2900 kmol s^{-1} (i.e., to the south), which can be compared with the estimated preindustrial transport into the Atlantic via the Bering Strait of about 1630 kmol s^{-1} [*Lundberg and Haugan*, 1996]. There therefore appears to have been a preindustrial (natural) divergence of the inorganic

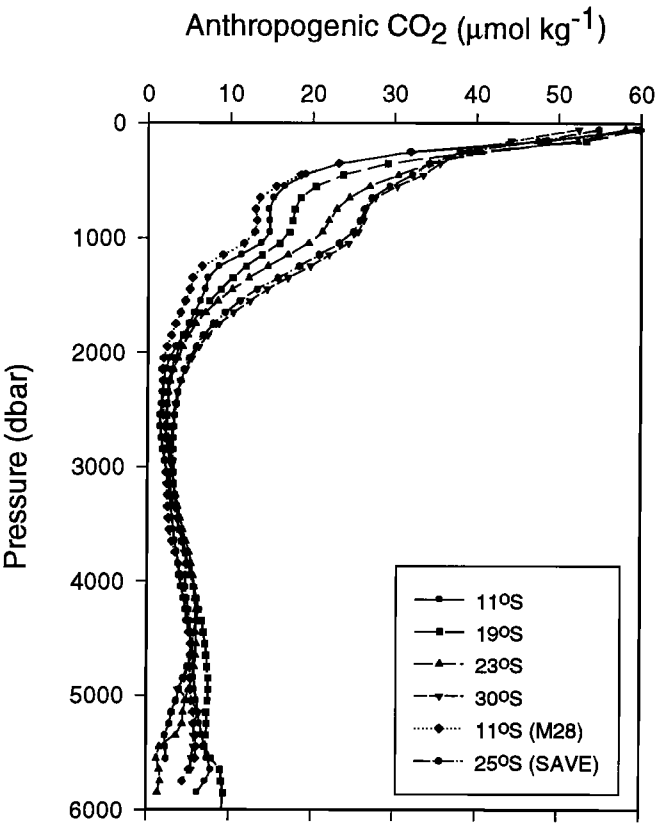

Figure 6. Average depth profile of anthropogenic CO_2 for the sections used during this study. Each profile represents the average profile for an entire section. (Note that most individual profiles had bottom depths shallower than 6000 m.)

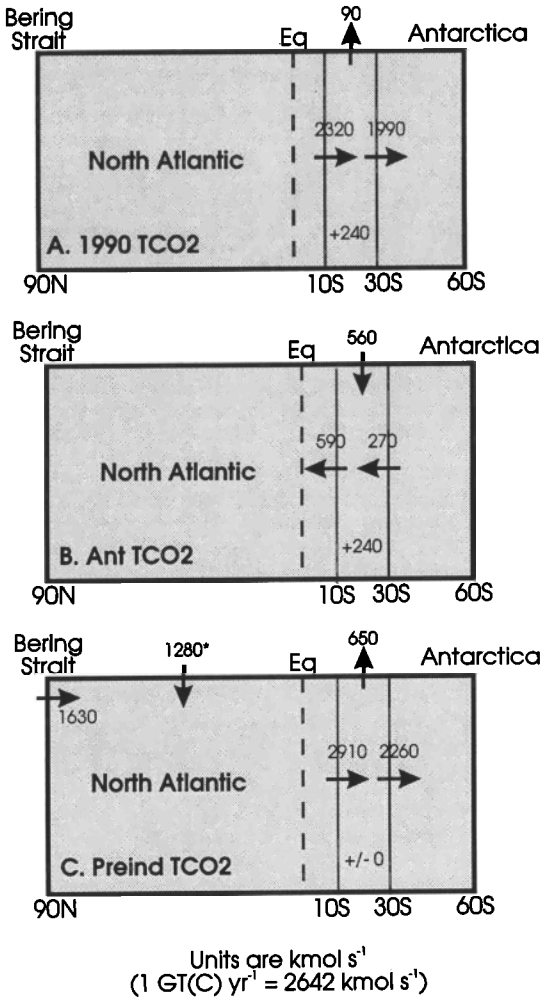

Figure 7. Schematic summary of the regional Atlantic Ocean inorganic carbon budget (10°S to 30°S) based on the water column transport and storage estimates. (a) the contemporary budget, (b) the budget for anthropogenic CO_2 , and (c) the preindustrial budget. The transport and storage units are kmol s^{-1} . The number +240 in Figures 7a and 7b refers to the storage term. In Figure 7c, the budget is extended to the North Atlantic, and the asterisked number at the top boundary refers to the combined effect of air-to-sea and riverine inorganic carbon fluxes.

carbon transport between Bering Strait and 10°S of the order of 1300 kmol s^{-1}, which was likely balanced by net air-to-sea transfer of CO_2 and riverine additions of inorganic carbon within the North Atlantic and Arctic Oceans (see Figure 7c). The potential role of organic carbon transports must also be considered in assessing this large-scale divergence [*Sarmiento et al.*, 1995].

6. Regional Carbon Budget (10°S - 30°S)

The carbon transport versus latitude data of Table 4 can be used to examine the regional inorganic carbon budget. Figure 7 summarizes the following discussion schematically for the contemporary, 1990s TCO_2 budget (Figure 7a), the anthropo-

Table 5. Summary of Approaches Used for Previously Published CO_2 Transport Estimates.

Paper	Transport Resolution		TCO_2 Data Resolution		Bering Strait?	(E-P)?	Remarks
	Vertical	Horizontal	Vertical	Horizontal			
Brewer et al. [1989]	23 layers	2 boxes	23 layers	five stations interpolated along isopycnals	no	no	mass transports from noncontemporaneous section
Broecker and Peng [1992]	2 layers	1 box	water-mass averages	water-mass averages	no	no	assumed overturning of 20 x 10^9 kg s^{-1}
Keeling and Peng [1995]	3-4 layers	1 box	water-mass averages	water-mass averages	no*	no	assumed overturning of 13 x 10^9 kg s^{-1}
Martel and Wunsch [1993]	11 layers	1° x 1°	11 layer (from MLR)	1° x 1° (from MLR)	no	yes	used direct current measurements, hydrography, and circulation model
Stoll et al. [1996]	50-200 m	25-50 km	50-200 m	25-50 km	yes	yes	did not resolve Canadian Archipelago and English Channel transports
This work	2-10 m	25-50 km	2-10 m (from MLR)	25-50 km (from MLR)	yes	yes	

The columns labeled "Bering Strait?" and "(E-P)?" refer to whether the calculations included adjustment of the mass transport across ocean sections in order to balance the salt transport via Bering Strait and/or the freshwater transport which is affected by runoff, evaporation (E), and precipitation (P) Barotropic velocities required to satisfy such constraints can carry significant carbon transports (see text) MLR is mixed-layer resolution

* Whereas *Keeling and Peng* [1992] did account for the contribution of water flowing through the Bering Strait to the PO_4 balance of the North Atlantic, they chose not to incorporate this transport component in their calculation of the cross-equatorial CO_2 transport

genic CO_2 budget (Figure 7b), and the preindustrial TCO_2 budget (Figure 7c).

A regression of T_C versus latitude (Figure 8a) indicates that the contemporary (i.e., 1990s) inorganic carbon transport decreased by 16.7 (±19) kmol s^{-1} per degree toward the south, implying a very slight convergence of 330 (±380) kmol s^{-1} between 10°S and 30°S (uncertainties are standard errors). Any contemporary convergence of inorganic carbon can be balanced by a sea-to-air flux of CO_2, net production of organic carbon, net dissolution of solid carbonates, and net storage of anthropogenic CO_2. (The regional river discharge as given by *Perry et al.* [1996] is $< 10^7$ kg s^{-1} which would carry a negligible inorganic carbon transport of < 10 kmol s^{-1}.) The magnitude of the anthropogenic carbon storage term can be estimated from the observed mean penetration depth (*MPD*) [*Broecker et al.*, 1979] for anthropogenic CO_2, which is defined as:

$$MPD = \frac{\int C_z \, dz}{C_{ml}} \qquad (10)$$

where C_{ml} and C_z are the concentrations of anthropogenic CO_2 in the mixed layer and at depth z, respectively. Using the ensemble of individual anthropogenic CO_2 profiles from each section, we estimated the *MPD* for anthropogenic CO_2 to be 770 m for the region between 10°S and 30°S. The uncertainty of this estimate may be of the order of 20% [cf. *Gruber et al.*, 1996]. *Gammon et al.* [1982] have shown that the vertical profile and *MPD* of a conservative tracer with a sea-surface concentration that is increasing exponentially with *e*-folding time of t years reaches a "transient steady state" after (3 x t) years [*Gammon et al.*, 1982]. Anthropogenic CO_2, which has been increasing exponentially since at least the mid-1800s with t = ~30 years, should by now have achieved transient steady state. Hence the storage or the inventory change of anthropogenic CO_2 during the 1990s can be estimated directly from the change in the mixed-layer concentration of anthropogenic CO_2 via (10). For the early 1990s, the surface concentration of anthropogenic CO_2 would have increased by 0.7 to 0.8 μmol kg^{-1} yr^{-1} in order to keep pace with the atmospheric pCO_2 increase of about 1.2 μatm yr^{-1}. This gives an average local storage rate of 0.59 (±20%) mol m^{-2} yr^{-1} or 240 (±49) kmol s^{-1} when integrated over the entire Atlantic Ocean surface area between 10°S and 30°S (12.8 x 10^{12} m^2).

This estimate, which is based on the framework of a vertical diffusion-advection model [*Gammon et al.*, 1982], can be tested against the directly observed buildup of anthropogenic CO_2 between the Geochemical Ocean Sections

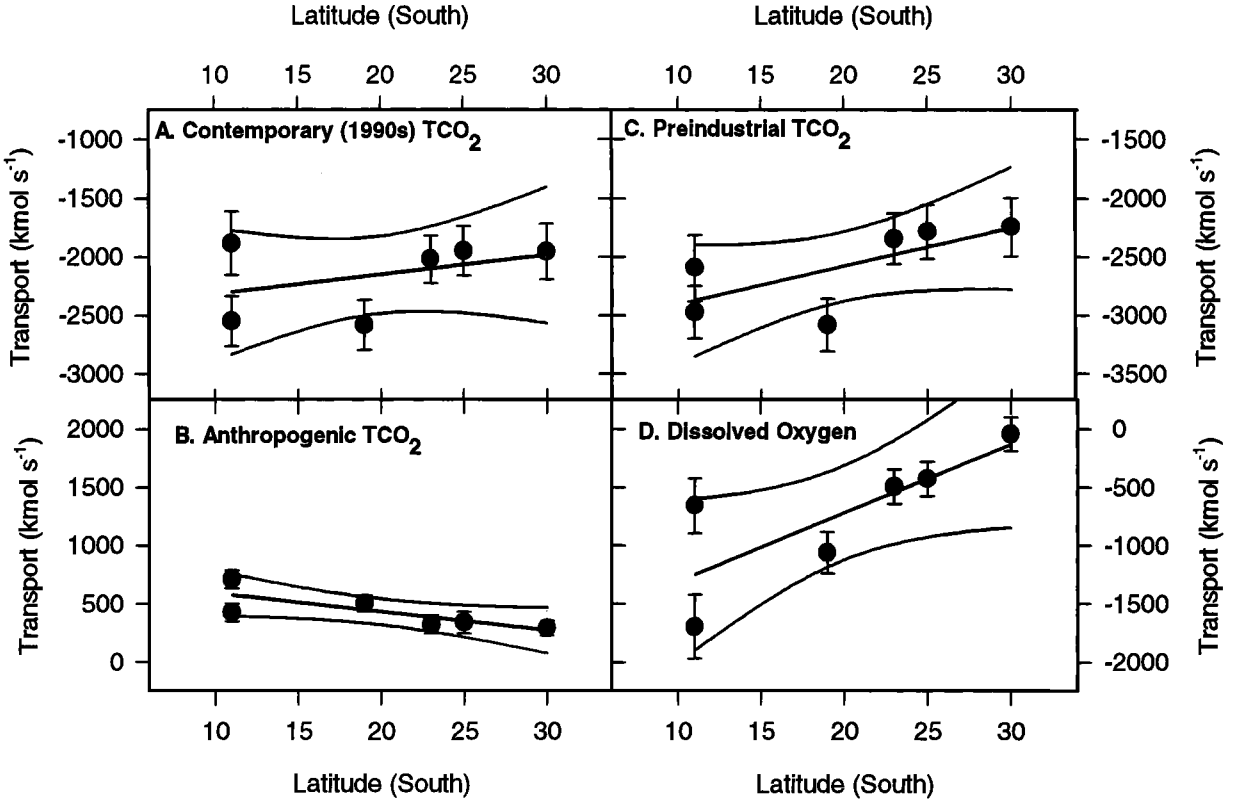

Figure 8. Mean transport versus latitude plots, with regression lines and 95% confidence intervals, based on the results presented in Table 4. Separate plots are presented for the following parameters: (a) the contemporary (1990s) inorganic carbon transport, (b) the anthropogenic carbon transport, (c) the preindustrial inorganic carbon transport, and (d) the dissolved oxygen transport. Note that the transport axis for each plot covers a total range of 2500 kmol s^{-1} and that the convention used is such that a negative transport denotes transport southward.

Study expedition of the mid-1970s and the WOCE expeditions of the 1990s. *Wallace et al.* [1996] conducted such an analysis for the western basin of the South Atlantic (5° - 35°S, west of 20°W) using a multivariate, time series analysis technique to compare the TCO_2 data collected during the two sampling periods. (Note that our data suggest that this more localized region has a mean penetration depth that is indistinguishable from the 10° - 30°S average.) On the basis of this empirical approach, the inventory change over 20 years is estimated to be 11.1 mol m^{-2} which gives a storage rate of 0.56 mol m^{-2}, identical to the one-dimensional model-derived estimate derived above.

The very slight convergence of inorganic carbon between 10°S and 30°S of 330 (±380) kmol s^{-1} in the contemporary ocean is therefore similar in magnitude to this anthropogenic carbon storage term. Further, the difference (90 ±380 kmol s^{-1}) between the contemporary inorganic carbon convergence and the anthropogenic carbon storage is reasonably consistent with a completely independent estimate of the net annual sea-to-air flux for this region of 264 kmol s^{-1} derived from surface pCO_2 data [*Takahashi et al.*, 1997]. The uncertainty of the latter estimate could be as high as 75%. This correspondence suggests that any additional net sources and sinks of inorganic carbon in this region, such as the local net production/respiration of organic carbon or dissolution of calcium carbonate, are not significantly different than zero (174 ± 400 kmol s^{-1}).

Figure 8b and Table 4 show that during the 1990s there was a significant ($p = 0.05$) divergence of the anthropogenic CO_2 transport between 10°S and 30°S amounting to ~320 (±128) kmol s^{-1}. An air-to-sea flux of anthropogenic CO_2 of 560 (±137) kmol s^{-1} would be required to balance the combined anthropogenic carbon storage and transport divergence terms, assuming no additional sources or sinks. In other words, the regional sea-to-air flux of CO_2 during the 1990s was approximately 560 kmol s^{-1} smaller than the corresponding sea-to-air flux of the preindustrial era.

Subtraction of the anthropogenic carbon transport from the contemporary transport implies a statistically significant ($p = 0.1$) local convergence of T_C between 11°S and 30°S for the preindustrial era (Table 4 and Figure 8c). During this period, we assume that the overall inorganic carbon inventory was in steady state (zero storage term), and if the biological productivity of the region was comparable to that of the contemporary ocean, the convergence would have been balanced by a considerable net sea-to-air flux of CO_2. The average preindustrial inorganic carbon convergence (32.6 ±17 kmol s^{-1} per degree of latitude) implies a total convergence of 650 (±340) kmol s^{-1} between 10°S and 30°S. Alternatively, taking *Takahashi et al.*'s [1997] estimate of 264 (±198) kmol s^{-1} for the contemporary sea-to-air flux of CO_2 (see above) and adding 560 (± 137) kmol s^{-1} to compensate for the air-to-sea transfer of anthropogenic CO_2 implies a preindustrial sea-to-air CO_2 flux of 824 (± 240) kmol s^{-1}. Once again, this is closely comparable to the preindustrial inorganic carbon convergence suggesting that local net production/respiration of organic carbon or dissolution of calcium carbonate was relatively small compared to the preindustrial sea-to-air flux.

Keeling and Peng [1995] have shown that the joint interpretation of meridional transports of both O_2 and CO_2 can distinguish the physical versus biological mechanisms responsible for the fluxes of these gases. As they point out, biologically driven fluxes of O_2 and CO_2 have opposite signs, whereas fluxes driven by thermal processes operate in the same direction. In this regard, our estimates of the meridional oxygen transport (Table 4 and Figure 8d) indicate convergence of the net southward O_2 transport, which we assume from direct transport estimates. In addition, the possible effects of seasonality on the convergence estimates require further examination.

7. Previous CO_2 Transport Estimates

There have been several earlier published attempts to estimate the meridional transport of inorganic carbon in the Atlantic Ocean. These used several different data sets, assumptions, and calculation procedures and are summarized in Table 5. A very important distinction between our transport estimates and many found in the earlier literature is our explicit incorporation of the net meridional mass transports required to satisfy salt and freshwater balances. *Stoll et al.* [1996] noted the significance of the CO_2 transport contribution which arises from net meridional mass transport through Bering Strait. They also noted that changes in the mass transport as a function of latitude, resulting from freshwater addition or removal, drive a significant meridional carbon transport divergence.

Following *Lundberg and Haugan* [1996] and *Stoll et al.* [1996], we have explicitly included this net mass transport in our estimates of the meridional CO_2 transport. This contribution was not, however, included in the CO_2 transport estimates given by *Brewer et al.* [1989] and *Broecker and Peng* [1992]. It was also not incorporated in transport estimates reported in preliminary meeting abstracts by *Holfort et al.* [1994] and *Robbins* [1994]. The latter was cited by *Sarmiento et al.* [1995] in their estimation of the inorganic carbon transport divergence between Bering Strait and the South Atlantic. *Martel and Wunsch* [1993] accounted for runoff, evaporation, and precipitation within their model domain (12°-60°N in the Atlantic Ocean) but apparently chose not to include the salt and mass transport through their model domain arising from the Bering Strait flow and runoff north of 60°N. *Keeling and Peng* [1995] accounted for the Bering Strait contribution to the North Atlantic phosphate balance but chose not to include its contribution to the total mass transport when calculating the inorganic carbon transport across the equator. Carbon cycle model simulations [e.g., *Sarmiento et al.*, 1995] do not always resolve this contribution because the transport through the Bering Strait is not always resolved.

To some extent, the choice of whether to include or ignore this contribution to the net carbon transport is a matter of philosophy and is contingent on the specific questions being asked of the transport estimates. One of the major reasons for examining carbon transport divergences is to obtain estimates of the regional distribution of the net air-sea flux of carbon (and oxygen). With this specific goal in mind, it is justifiable to ignore the inorganic carbon transport which is tied to the net salt transport across sections. This component of the inorganic carbon transport, while large, can be viewed as constant across all Atlantic sections and therefore does not affect or reflect the air-sea flux of CO_2 or O_2. However, if direct comparisons are made with the net transport of inorganic carbon through the Bering Strait, such as were made by

Sarmiento et al. [1995], then it is essential that the contribu- should not have changed since the preindustrial era. The observation that the transport of both gases in the preindustrial ocean was convergent is qualitatively consistent with a thermal forcing mechanism driving the efflux of both O_2 and CO_2 across the air-sea interface in this region.

Our heat transport calculations (Table 4) indicate significant ($p < 0.1$) divergence of the northward heat transport between 10°S and 30°S averaging 0.012 ($\pm$ 0.006) x 10^{15} W per degree of latitude, implying addition of heat to the water column. *Watson et al.* [1995] have estimated the maximum air-sea CO_2 flux driven by the heat transport of the North Atlantic ocean to be ~0.75 Gt *C* yr^{-1} or ~2000 kmol s^{-1} of CO_2 uptake for each petawatt (10^{15} W) of northward heat transport. Applying their scaling to our observed divergence of the northward heat transport between 10°S and 30°S (Table 4) gives a maximum thermally driven CO_2 sea-to-air flux of (2000 x 20 x 0.012) or 480 ($\pm$ 240) kmol s^{-1}, which is quite consistent with the observed preindustrial inorganic carbon convergence and estimated preindustrial sea-to-air flux of CO_2 (see above). A similar calculation for dissolved oxygen gives a maximum sea-to-air O_2 flux of ~1500 kmol s^{-1} PW^{-1} of heat transport divergence, which implies a maximum thermally driven sea-to-air O_2 flux of (1500 x 20 x 0.012) or 360 ($\pm$ 180) kmol s^{-1} for the same latitude range. The observed convergence of oxygen, however, was 1180 ($\pm$460) kmol s^{-1} between 10°S and 30°S.

Hence the observed convergence of both gases is qualitatively consistent with the sign of the observed heat transport divergence. In the case of CO_2, the magnitude of the convergence is also quantitatively consistent with the maximum that would be predicted theoretically from the observed heat flux divergence, whereas for dissolved oxygen the observed convergence is 2-3 times the theoretical prediction. Given that air-sea equilibration of O_2 is an order of magnitude more rapid than that of CO_2, it is perhaps not surprising that gas exchange would create a stronger convergence signal for O_2 than for CO_2. However, an observed oxygen convergence larger than that predicted on the basis of the observed heat flux divergence is harder to explain except as the result of (1) uncertainty in the various transport and convergence estimates themselves (note the large error bars for the convergence estimates and, particularly, the possible influence of seasonality of the transports, section 4.3); (2) violation of the assumption of no storage for dissolved oxygen; or (3) an "extra" contribution to a predominantly thermally driven convergence arising from some biological mechanism (e.g., a divergence of the organic carbon transport).

On balance, the qualitative picture is consistent with independent estimates of the air-sea CO_2 flux, and the overall budget for preindustrial carbon suggests a relatively minor role for biologically driven convergence/divergence in this particular region. However, it should be clear from the above that measurements of the total organic carbon concentration of seawater, which were unfortunately not available for the sections used in this study, would provide independent constraints on the air-sea CO_2 exchange scenarios inferred tion of this component of the transport be included in the transport estimates at all latitudes.

Of potentially more significance is the effect of net freshwater addition or removal via runoff or evaporation and precipitation, which can significantly affect the divergence of the net meridional mass transport [*Stoll et al.*, 1996] and which must be accounted for when estimating carbon transport divergences. As noted by *Stoll et al.* [1996], the pioneering analysis by *Brewer et al.* [1989] was based on an assumption of zero net meridional mass transport and therefore did not include this effect.

Contrary to a statement by *Stoll et al.* [1996], the CO_2 transport estimates of *Broecker and Peng* [1992] and *Keeling and Peng* [1995] do implicitly correct for this effect by normalizing the observed inorganic carbon concentrations to constant salinity. Through this normalization, the addition of variable levels of freshwater to different water masses (and hence dilution of inorganic carbon) is compensated for. In principle, this correction should serve the same purpose as keeping track of the freshwater transport divergence; however, in practice, the efficacy of this "normalization" approach has not been independently verified. That is, as it was applied, did the salinity normalization reflect a reasonable freshwater transport distribution? In contrast, we have chosen to explicitly consider the salt, freshwater, and carbon transports rather than calculating the transport of salinity-normalized quantities. Using a measurement-based salt transport constraint, estimated baroclinic, Ekman, and barotropic transports, and the observed salinity distribution, we were able to directly estimate the freshwater transport divergence. This was consistent with independent estimates of this quantity [*Baumgartner and Reichel*, 1975] (see section 4.4) thereby increasing our confidence that the freshwater transport divergence is being correctly represented when estimating the inorganic carbon transport divergence.

This discussion emphasizes the wide variety of approaches and philosophies that have been promulgated in order to calculate carbon transports. Not surprisingly, this variety has led to confusions of interpretation and a risk of comparing unlike transport estimates. It is therefore important to reiterate that we have reported the total net transport of inorganic carbon across the South Atlantic sections. These estimates incorporate the carbon transport associated with a net mass flow through a section which is required to balance the salt input through Bering Strait. They therefore also reflect the meridionally varying mass transport which is associated with freshwater addition and removal.

Table 5 highlights some other ways in which our approach to calculating inorganic carbon transport differs from prior estimates. Notably, our estimate is based on a very large, high-quality data set, including four sections of TCO_2 data which have been interpolated onto the CTD data using multiple regression. Many of the earlier estimates were based on limited data sets, often relying on bulk average concentrations for different water masses or layers. Several analyses have relied on bulk overturning calculations in which the net mass flux in an upper layer and a deep layer are multiplied by zonally averaged property concentrations for the respective layers. The potential risks associated with estimates that are based on smoothed fields are discussed in detail by *Rintoul and Wunsch* [1991], who found that accurate estimates of nutrient transports can require very detailed estimates of the circulation and property fields.

We examined the difference between the T_C calculated using our full inverse model solutions and that derived from

a zonally averaged estimate of the transport for the *Meteor* 28 (11°S) and *Meteor* 22 (30°S) sections. For the zonally averaged T_C, we calculated the sum, over all 19 vertical layers in the model, of the product of a layer-average net mass transport and a layer-average TCO_2 concentration. At 30°S, the zonally averaged solution was only 100-250 kmol s^{-1} (10%) different from the full model solution. However, at 11°S the zonally averaged solution was almost 1000 kmol s^{-1} or 50% lower than the full solution. Inspection of the solutions suggested that the large difference at 11°S was the result of a strong western boundary subsurface current in the depth range 50-800 m at that latitude [cf. *Schott et al.*, 1995] coupled with a large difference in TCO_2 concentration between the western and eastern boundaries.

We also compared the T_C derived from the full inverse model solutions with that derived from a two-layer zonally averaged overturning calculation similar to that used by *Broecker and Peng* [1992] and *Keeling and Peng* [1995]. We defined the upper layer as $\sigma_2 < 36.8$ and defined the lower layer as $\sigma_2 > 36.8$. The magnitude of the overturning circulation implied by these calculations ranged from 11 to 14 x 10^9 kg s^{-1}, which is close to that assumed by *Keeling and Peng* [1995] but much lower than the 20 x 10^9 kg s^{-1} assumed by *Broecker and Peng* [1992]. As with the zonally averaged solution discussed above, at 30°S the simple overturning calculation gave transports which were only 200-300 kmol s^{-1} (10-15%) lower than the full model solution. However, at 11°S the overturning calculation gave a transport which was 700-900 kmol s^{-1} or ~40% lower than that derived using the full model. Obviously, caution must be exercised when attempting to estimate the transport of inorganic carbon; under certain circumstances it appears that simple averaging of the velocity and concentration fields can provide accurate carbon transports. However, in other circumstances such simplified calculations may be subject to large errors.

Our analysis shares many similarities with the work of *Stoll et al.* [1996], who estimated the CO_2 transport across a single section between Greenland and Ireland. Our analysis benefits from having been able to sample the boundary currents, whereas ice precluded Stoll et al. from sampling within the East Greenland Current. Our multiple zonal sections also allow for a more detailed inverse analysis. The South Atlantic sections benefit from being closed, whereas the section occupied by *Stoll et al.* [1996] could not explicitly address transport via the Canadian Arctic Archipelago, the English Channel, and the Irish Sea. For example, *Lundberg and Haugan* [1996] estimate the net mass transport through the Canadian Archipelago to be 1.4 x 10^9 kg s^{-1} with a mean TCO_2 concentration of ~2070 μmol kg^{-1}. This implies a nonnegligible transport of ~3000 kmol s^{-1} via this route. Sections which resolve this transport pathway (e.g., sections across the Labrador Sea) should be incorporated into any future inverse analysis of net inorganic carbon transport within the northern North Atlantic.

8. Summary

The transport of inorganic carbon across six zonal sections occupied between 11°S and 30°S in the South Atlantic Ocean has been estimated. During the early 1990s, the transport was directed southward, decreased slightly toward the south, and was -2150 ± 200 kmol s^{-1} across 20°S. This transport includes a large contribution associated with a barotropic velocity required to satisfy the salt flux constraint measured at the Bering Strait. While estimation of this contribution is not essential for assessing the inorganic carbon uptake by the North Atlantic overturning circulation and was not incorporated into several earlier estimates of ocean carbon transport, it is critical for assessing the ocean carbon transport divergence between the Bering Strait and the South Atlantic. The principal sources of uncertainty in the transport estimates originate with the Ekman component of the transport, particularly at low latitudes, together with uncertainties in determining the barotropic component of the velocity field. The barotropic transport uncertainty was reduced through use of an inverse model and could probably be reduced further by the use of more sophisticated inverse calculations and additional constraints. To lower the uncertainty in the Ekman transport, a better knowledge of the annual wind stress will be required. A better understanding of the effects of seasonal variations of the carbon transport is required.

By estimating the anthropogenic component of the TCO_2 distribution, it was shown that there was a net northward transport of anthropogenic carbon across 20°S of 430 kmol s^{-1}. This transport increased toward the north. By difference, the preindustrial southward transport of inorganic carbon across 20°S was -2580 kmol s^{-1}. The preindustrial transports show net convergence of both CO_2 and O_2 between 10°S and 30°S, suggesting that this region was a net source of both gases for the atmosphere during the preindustrial era, consistent with thermal forcing of the gas flux. Our transport estimates also suggest that transport of anthropogenic carbon by the upper limb of the meridional overturning circulation may supply a significant fraction of the anthropogenic CO_2 which is currently being stored within the North Atlantic Ocean.

Appendix

The constraints used in the inverse model analysis were as follows:

1. The total salt transport across the South Atlantic zonal sections is 26.7 x 10^6 kg s^{-1}. This constraint is based on the salt transport through the Bering Strait and the assumption of a steady state salt balance within the North Atlantic. Note that this is a departure from the more commonly used constraint of net mass transport used for heat transport calculations.
2. Salt is conserved in boxes bounded by the different sections and/or the continents in the horizontal plane and by specified density surfaces in the vertical plane. The vertical layers include those used by *MacDonald* [1993] and *Roemmich* [1983] and are listed in the caption to Figure 4.
3. There is no net meridional flow within layers deeper than 3000 dbar in the eastern basin of the South Atlantic because of the blocking of such flows by the Walvis and Mid-Atlantic Ridges.
4. The transport of the Brazil current at 30°S (vertical extent of 0-600 m) is taken to be 10 x 10^9 kg s^{-1} southward, and the flow of Antarctic Bottom Water ($\sigma_4 > 45.92$) through the Vema Channel is 5 x 10^9 kg s^{-1} northward. The

values of these transports were determined from direct current measurements [*Holfort*, 1994; Holfort et al., manuscript in preparation, 1998).

5. *Keeling and Peng* [1995] applied the constraint that the net meridional transport of phosphate across the equator should equal the phosphate transport through Bering Strait (about 1.7 kmol s^{-1}). Use of a similar constraint in our inverse calculation significantly restricted the range of valid solutions and better constrained the heat, water and carbon transports, while only slightly altering their mean values (Holfort et al., manuscript in preparation, 1998). However, it is probably more appropriate to assume a balance for total phosphorus in the Atlantic, which suggests that the transport of organic phosphorus must also be considered. There are surprisingly few measures of total phosphorus in the open ocean, yet dissolved organic forms of phosphorus constitute 50-100% of the phosphorus in the ocean's surface layer. Measurements at the Hawaii Ocean Time Series Site [e.g., *Karl and Tien*, 1997] show dissolved organic phosphorus concentrations of 0.1 - 0.3 μmol kg^{-1} within the upper 500 m, dropping to <0.05 μmol kg^{-1} below 1000 m. If such levels are typical of the South Atlantic, there is a potential net northward transport of organic phosphorus of the order of 10 x 10^9 kg s^{-1} x 0.25 μmol kg^{-1} or 2.5 kmol s^{-1} associated with transport within the upper layers of the ocean. This is presumably balanced by a net southward transport of inorganic phosphorus (phosphate) which is in addition to the phosphate transported through the Bering Strait. Without data on the concentration of organic phosphorus, there is considerable uncertainty in how to exactly specify the phosphate transport constraint. Hence during the inverse analysis, three separate variants of the phosphate transport constraint were applied which bound a reasonable set of possibilities: (1) The phosphate transport was specified to be identical across all of the South Atlantic sections, but its magnitude was not specified. The phosphate transport which resulted from applying this variant of the constraint was generally between 4 and 8 kmol s^{-1} southward. (2) A phosphate transport of 2 kmol s^{-1} southward across all sections was specified (very similar to the constraint used by *Keeling and Peng* [1995]). (3) A net phosphate transport of 4 kmol s^{-1} southward across all sections was assumed in order to balance the likely net northward transport of organic phosphorus as well as the Bering Strait input.

For the results presented in this paper, most weight was assigned to the 4 kmol s^{-1} constraint.

Acknowledgments. This work was supported by the U.S. Department of Energy (Office of Biological and Environmental Research) under contract DE-AC02-98CH00016 and by the German Ministry of Science and Technology (BMBF). The support of Michael Riches of DOE in allowing us to complete this analysis is acknowledged. The authors benefitted from discussions with and input from Charlie Flagg, Alfred Putzka, Paul Robbins, Ralph Keeling, Ernie Lewis, Jorge Sarmiento, Scott Doney, Rik Wanninkhof, and the DOE CO_2 Survey Science Team. Assistance with data collection from Rick Wilke, Craig Neill, and the scientists and crew of the *Meteor* is gratefully acknowledged. We particularly thank Taro Takahashi and David Chipman for generously providing access to their excellent SAVE data set. This is a WOCE and JGOFS contribution.

References

Anderson, L. G., D. Dyrssen, and E. P. Jones, An assessment of the transport of atmospheric CO_2 into the Arctic Ocean, *J. Geophys. Res.*, *95*, 1703-1711, 1990.

Baumgartner, A., and E. Reichel, *Die Weltwasserbilanz*, 197 pp., Oldenburg, Munich, Germany, 1975.

Bates, N. R., A. F. Michaels, and A. H. Knap, Seasonal and interannual variability of oceanic carbon dioxide species at the U.S. JGOFS Bermuda Atlantic Time-Series Study (BATS) Site, *Deep-Sea Res., II, 43*, 347-383, 1996.

Boebel, O., C. Schmidt, and W. Zenk, Flow and recirculation of Antarctic Intermediate Water across the Rio Grande Rise, *J. Geophys. Res., 102*, 20967-20986, 1997.

Brewer, P. G., Direct observation of the oceanic CO_2 increase, *Geophys. Res. Lett., 5*, 997-1000, 1978.

Brewer, P. G., and J. C. Goldman, Alkalinity changes generated by phytoplankton growth, *Limnol. Oceanogr., 21*(1), 108-117, 1976.

Brewer, P. G., C. Goyet, and D. Dyrssen, Carbon dioxide transport by ocean currents at 25°N latitude in the Atlantic Ocean, *Science, 246*, 477-479, 1989.

Brewer, P. G., D. M. Glover, C. Goyet, and D. K. Shafer, The pH of the North Atlantic Ocean: Improvements to the global model for sound adsorption in seawater, *J. Geophys. Res., 100*, 8761-8776, 1995.

Broecker, W. S., and T.-H. Peng, Interhemispheric transport of carbon dioxide by ocean circulation, *Nature, 356*, 587-589, 1992.

Broecker, W. S., T. Takahashi, H. J. Simpson, and T.-H. Peng, Fate of fossil fuel carbon dioxide and the global carbon budget, *Science, 206*, 409, 1979.

Bryan, K., Measurements of meridional heat transport by ocean currents, *J. Geophys. Res., 67*, 3403-3414, 1962.

Chen, C.-T. A., and F. J. Millero, Gradual increase of oceanic CO_2, *Nature, 277*, 205-206, 1979.

Coachman, L. K., and K. Aagard, Transports through Bering Strait: Annual and interannual variability, *J. Geophys. Res., 93*, 15535-15539, 1988.

Conway, T. J., P. P. Tans, and L. S. Waterman, Atmospheric CO_2 records from sites in the NOAA/CMDL air sampling network, in *Trends '93: A Compendium of Data on Global Change*, edited by T. A. Boden et al., *Rep. ORNL/CDIAC-65*, pp. 41-119, Carbon Dioxide Inf. and Anal. Cent., Oak Ridge Nat. Lab., Oak Ridge, Tenn., 1994.

Dickson, R., J. Lazier, J. Meincke, P. Rhines, and J. Swift, Long-term coordinated changes in the convective activity of the North Atlantic, *Prog. Oceanogr., 38*, 241-295, 1997.

Enting, I. G., C. M. Trudinger, and R. J. Francey, A synthesis inversion of the concentration and $\delta^{13}C$ of atmospheric CO_2, *Tellus, Ser. B, 47*, 35-52, 1995.

Fu, L.-L., The general circulation and meridional heat transport of the subtropical South Atlantic determined by inverse methods, *J. Phys. Oceanogr., 11*, 1171-1193, 1981.

Gammon, R.H., J. Cline, and D. Wisegarver, Chlorofluoromethanes in the northeast Pacific Ocean: Measured vertical distributions and application as transient tracers of upper ocean mixing. *J. Geophys. Res., 87*, 9441-9454, 1982.

Goyet, C., and D. Davis, Estimation of total CO_2 concentration throughout the water column, *Deep Sea Res., Part I, 44*, 859-877, 1997.

Goyet, C., D. Davis, E. T. Peltzer, and P. G. Brewer, Development of improved space sampling strategies for ocean chemical properties: Total carbon dioxide and dissolved nitrate, *Geophys. Res. Lett., 22*, 945-948, 1995.

Gruber, N., J. L. Sarmiento, and T. F. Stocker, An improved method for detecting anthropogenic CO_2 in the oceans, *Global Biogeochem. Cycles, 10*(4), 809-837, 1996.

Hall, M., and H. L. Bryden, Direct estimates and mechanisms of ocean heat transport, *Deep Sea Res., Part A, 29*, 339-359, 1982.

Hellermann, S., and M. Rosenstein, Normal monthly wind stress over the world ocean with error estimates, *J. Phys. Oceanogr., 13*, 1093-1104, 1983.

Holfort, J., Grossräumige zirkulation und meridionale transporte im

Südatlantik, *Ber. Inst. Meereskd. Christian Albrechts Univ. Kiel, 260*, 1994.

Holfort, J., K. M. Johnson, D. W. R. Wallace, and B. Schneider, Meridional transport of total dissolved inorganic carbon in the South Atlantic Ocean (abstract), *Eos Trans. AGU, 75*(3), Ocean Sci. Meet. Suppl., 161, 1994.

Isemer, H. J., and L. Hasse, *The Bunker Climate Atlas of the North Atlantic Ocean,* Vol. 2, *Air-Sea Interactions*, 252 pp., Springer Verlag, New York, 1985.

Johnson, K.M., and D. W. R. Wallace, The single-operator multiparameter metabolic analyzer for total carbon dioxide with coulometric detection, *DOE Res. Summ., 19,* Carbon Dioxide Inf. Anal. Cent., Oak Ridge Nat.Lab., Oak Ridge, Tenn., 1992.

Johnson, K. M., K. D. Wills, D. B. Butler, W. K. Johnson, and C. S. Wong, Coulometric total carbon dioxide analysis for marine studies: Maximizing the performance of an automated gas extraction system and coulometric detector, *Mar. Chem., 44*, 167-187, 1993.

Johnson, K. M., D. W. R. Wallace, R. J. Wilke, and C. Goyet, Carbon dioxide, hydrographic, and chemical data obtained during the R/V *Meteor* cruise in the South Atlantic Ocean (WOCE section A9, February-March 1991), *Publ. 4416,* Carbon Dioxide Inf. Anal. Cent., Oak Ridge Nat. Lab., Oak Ridge, Tenn., 1995.

Johnson, K. M., B. Schneider, L. Mintrop, and D. W. R. Wallace, Carbon dioxide, hydrographic, and chemical data obtained during the R/V *Meteor* cruise 22/5 in the South Atlantic Ocean (WOCE section A10, December 1992 - January 1993), *Publ.*, Carbon Dioxide Inf. Anal. Cent., Oak Ridge Nat. Lab., Oak Ridge, Tenn., in press, 1998.

Josey, S. A., E. C. Kent, D. Oakley, and P. K. Taylor, A new global air-sea heat and momentum flux climatology, *Int. WOCE Newslett., 24*, 3-5, 1996.

Karl, D. M., and G. Tien, Temporal variability in dissolved phosphorus concentrations in the subtropical North Pacific Ocean, *Mar. Chem., 56,* 77-96, 1997.

Keeling, C. D., R. B. Bacastow, A. F. Carter, S. C. Piper, T. P. Whorf, M. Heimann, W. G. Mook, and H. Roeloffzen, A three-dimensional model of atmospheric CO_2 transport based on observed winds, *Ser.,* 1, Analysis of observational data, in *Aspects of Climate Variability in the Pacific and the Western Americas*, *Geophys. Monogr.* vol. 55, edited by D.H. Peterson, pp. 165-236, AGU, Washington, D.C., 1989.

Keeling, R. F., and T.-H. Peng, Transport of heat, CO_2 and O_2 by the Atlantic's thermohaline circulation, *Philos. Trans. R. Soc. London, Ser. B, 348,* 133-142, 1995.

Lundberg, L., and P. M. Haugan, A Nordic Seas - Arctic Ocean carbon budget from volume flows and inorganic carbon data, *Global Biogeochem. Cycles, 10*(3), 493-510, 1996 .

MacDonald, A. M., Property fluxes at 30°S and their implications for the Pacific-Indian throughflow and the global heat budget, *J. Geophys. Res., 98,* 6851-6868, 1993.

MacDonald, A. M., and C. Wunsch, Oceanic estimates of global ocean heat transport, in *US WOCE Implementation Report, Rep. 8*, pp. 28-30, Texas A&M Univ., College Station, Tex., July 1996.

Martel, F., and C. Wunsch, The North Atlantic Circulation in the early 1980's - An estimate from inversion of a finite-difference model, *J. Phys. Oceanogr., 23,* 898-924, 1993.

Neftel, A. E., E. Moor, H. Oeschger, and B. Stauffer, Evidence from polar ice cores for the increase of atmospheric CO_2 in the past two centuries, *Nature, 315,* 45-47, 1985.

Perry, G. D., P. B. Duffy, and N. L. Miller, An extended data set of river discharges for validation of general circulation models, *J. Geophys. Res., 101*, 21339-21349, 1996.

Reid, J. L., On the total geostrophic circulation of the South Atlantic Ocean: Flow patterns, tracers and transports, *Prog. Oceanogr.*, 23, 149-244, 1989.

Rintoul, S. R., and C. Wunsch, Mass, heat, oxygen and nutrient fluxes and budgets in the North Atlantic Ocean, *Deep Sea Res., 38,* suppl. 1, S355-S377, 1991.

Robbins, P. E., Direct observations of the meridional transport of total inorganic carbon in the south Atlantic Ocean (abstract), *Eos Trans.* AGU, *75*(3), Ocean Sci. Meet. Suppl., 161, 1994.

Robbins, P.E., and H. L. Bryden, Direct observations of advective nutrient and oxygen fluxes at 24° N in the Pacific Ocean, *Deep Sea Res., Part I, 41*, 143-168, 1994.

Roemmich, D., Estimation of meridional heat flux in the North Atlantic by inverse methods, *J. Phys. Oceanogr., 10,* 1972-1983, 1980.

Roemmich, D., The balance of geostrophic and Ekman transports in the tropical Atlantic Ocean, *J. Phys. Oceanogr., 13,* 1534-1539, 1983.

Roemmich, D., and C. Wunsch, Two transatlantic sections: meridional circulation and heat flux in the subtropical North Atlantic Ocean, *Deep Sea Res., Part A, 32,* 619-664, 1985.

Roether, W., and A. Putzka, Transient-tracer information on ventilation and transport of South Atlantic Waters, in *The South Atlantic: Present and Past Circulation*, edited by G. Wefer et al., pp. 45-62, Springer-Verlag, New York, 1996.

Sabine, C. L., D. W. R. Wallace, and F. J. Millero,. Survey of CO_2 in the oceans reveals clues about global carbon cycle, *Eos Trans.* AGU, *78*(5), 49, 54-55, 1997.

Sarmiento, J. L., R. Murnane, and C. le Quéré, Air-sea CO_2 transfer and the carbon budget of the North Atlantic, *Philos. Trans. R. Soc. London, Ser. B, 348,* 211-219, 1995.

Saunders, P. M. and B. A. King, Oceanic fluxes on the WOCE A11 section, *J. Phys. Oceanogr., 25*(9), 1942-1958, 1995.

Schott, F., L. Skamma, and J. Fischer, The warm water inflow into the western tropical Atlantic boundary region, spring 1994, *J. Geophys. Res., 100,* 24745-24760, 1995.

Siedler, G., and W. Zenk, WOCE Südatlantik 1991, Reise Nr. 15, 30. Dezember 1990 - 23 März 1991, *METEOR-Ber., 92-1*, 126 pp., Univ. Hamburg, Hamburg, Germany, 1992.

Siedler, G., W. Balzer, T. J. Müller, R. Onken, M. Rhein, and W. Zenk, WOCE South Atlantic 1992, Cruise No. 22, 22 September 1992 - 31 January 1993, *METEOR-Ber., 93-5*, 131 pp., Univ. Hamburg, Hamburg, Germany, 1993.

Siedler, G., T. J. Mueller, R. Onken, M. Arhan, H. Mercier, B. A. King, and P. M. Saunders, The zonal WOCE sections in the South Atlantic, in *The South Atlantic: Present and Past Circulation*, edited by G. Wefer et al., pp. 83-104, Springer-Verlag, New York, 1996.

Stoll, M. H. C., H. M. van Aken, H. J. W. deBaar, and C. J. deBoer, Meridional carbon dioxide transport in the northern North Atlantic, *Mar. Chem., 55,* 205-216, 1996.

Takahashi, T., R. A. Feely, R. Weiss, R. Wanninkhof, D. W. Chipman, S. C. Sutherland, and T. T. Takahashi, Global air-sea flux of CO_2: An estimate based on measurements of sea-air $pCO2$ difference, in *NAS Colloquium Volume on Carbon Dioxide and Climate Change*, edited by C.D. Keeling, pp. 8292-8299, *Natl. Acad. Sci.*, Washington, D.C., 1997.

Tans, P. P., I. Y. Fung, and T. Takahashi, Observational constraints on the global atmospheric CO_2 budget, *Science, 247,* 1431-1438, 1990.

Wallace, D. W. R., Monitoring global ocean carbon inventories, report, 54 pp., Ocean Obs. Syst. Dev. Panel, Tex. A&M Univ., College Station, Tex., 1995.

Wallace, D. W. R., P. Beining, and A. Putzka, Carbon tetrachloride and chlorofluorocarbons in the South Atlantic Ocean, 19°S, *J. Geophys. Res., 99*, 7803-7819, 1994.

Wallace, D. W. R., K. M. Johnson, J. Holfort, and B. Schneider, Detection of the changing CO_2 inventory in the ocean, in *1996 U.S. WOCE Report, U.S. WOCE Implement. Rep. 8*, pp. 31-33, U.S. World Ocean Circ. Exp. Office, Dept. of Oceanogr., Tex. A&M Univ., College Station, Tex., 1996.

Watson, A. J., P. D. Nightingale, and D. J. Cooper, Modelling atmosphere-ocean CO_2 transfer, *Philos. Trans. R. Soc. London, Ser. B, 348*, 125-132, 1995.

Wunsch, C., The North Atlantic general circulation west of 50°W determined by inverse methods, *Rev. Geophys., 16,* 583-620, 1978.

Wunsch, C., D. Hu, and B. Grant, Mass, heat, salt and nutrient fluxes in the South Pacific Ocean,. *J. Phys. Oceanogr., 13*, 725-753. 1983.

Zenk, W. and T. J. Müller, WOCE studies in the South Atlantic, Cruise No. 28, 29 March - 14 June 1994, *METEOR-Ber., 95-1* 193 pp., Univ. Hamburg, Hamburg, Germany, 1995.

D.W.R. Wallace, Brookhaven National Laboratory, PO Box 5000 Dept. of Applied Science, Upton, NY 11973-5000 (e-mail wallace@bnl.gov)

J. Holfort, Brookhaven National Laboratory, PO Box 5000, Dept. of Applied Science, Upton, NY 11973-5000

(Received October 14, 1997, revised, April 22, 1997; accepted May 1, 1998.)